

NASA Technical Memorandum 101606

An LQR Controller Design Approach for a Large Gap Magnetic Suspension System (LGMSS)

Nelson J. Groom and
Philip R. Schaffner

(NASA-TM-101606) AN LQR CONTROLLER DESIGN
APPROACH FOR A LARGE GAP MAGNETIC SUSPENSION
SYSTEM (LGMSS) (NASA) 65 D CSCL 13B

N90-29751

Unclas
G3/31 0304531

July 1990



National Aeronautics and
Space Administration

Langley Research Center
Hampton, VA 23665



SUMMARY

Two control approaches for a Large Gap Magnetic Suspension System (LGMSS) are investigated and numerical results are presented. The approaches are based on Linear Quadratic Regulator (LQR) control theory and include a nonzero set point regulator with constant disturbance input and an integral feedback regulator. The LGMSS provides five degree-of-freedom control of a cylindrical suspended element which is composed of permanent magnet material. The magnetic actuators are air core electromagnets mounted in a planar array.

INTRODUCTION

This paper describes two control approaches for a Large Gap Magnetic Suspension System (LGMSS). The approaches are based on LQR control theory and include a nonzero set point regulator with constant disturbance input and an integral feedback regulator. The LGMSS is a conceptual design for a ground-based experiment which could be used to investigate the technology issues associated with magnetic suspension at large gaps, accurate suspended element control at large gaps, and accurate position sensing at large gaps. This technology would be applicable to future efforts which could range from magnetic suspension of wind tunnel models to advanced spacecraft experiment isolation and pointing systems. The LGMSS provides five degree-of-freedom control. The suspended element is a cylinder which is composed of permanent magnet material and the magnetic actuators are air core electromagnets mounted in a planar array. This configuration is described and an analytical model developed in reference 1. Values of magnetic fields generated by the electromagnets at the location of the suspended core are presented and the method of calculation discussed in Appendix A which was written by Colin P. Britcher, Department of Mechanical Engineering and Mechanics, Old Dominion University, Norfolk, Virginia. All numerical results which are presented were obtained by using MATRIX_χ with SYSTEM_BUILD.¹ The MATRIX_χ implementation of the system is presented in Appendix B. Numerical results were obtained for positioning accuracy, with fixed gains, over large angular displacements about the yaw axis.

LGMSS ANALYTICAL MODEL

This section presents an analytical model of the LGMSS. For a detailed development of the model see reference 1. The suspended element, or core, is a cylinder which is composed of permanent magnet material. The core is suspended over a planar array of five electromagnets mounted in a circular configuration. Figure 1 is a schematic representation of this system which shows the coordinate systems and initial alignment. A set of orthogonal \bar{x} , \bar{y} , \bar{z} , body fixed axes defines the motion of the core with respect to inertial space. The core coordinate system is initially aligned with an orthogonal x , y , z system fixed in inertial space. A set of orthogonal x_b , y_b , z_b axes, also fixed in inertial space, define the location of the electromagnet array with respect to the x , y , z system. The x_b and y_b axes are parallel to the x and y axes respectively and the z_b and z axes are aligned. The centers of the two axis-systems are separated by the distance h . The angular acceleration of the core, in core coordinates, can be written as (see ref. 1)

$$\{\ddot{\bar{\Omega}}\} = (1/I_c) (\text{Vol}([\bar{M}][T_m]\{B\}) + \{\bar{T}_d\}) \quad (1)$$

where I_c is the core moment of inertia about the axes of symmetry (y and z), Vol is the volume of the core, \bar{M} is the magnetization of the core, $[\bar{M}]$ is the skew symmetric cross product matrix, $[T_m]$ is the vector transformation matrix from inertial to core coordinates, $\{B\}$ is the flux density produced by the

¹Use of names of products in this report does not constitute an official endorsement of such products, either expressed or implied, by the National Aeronautics and Space Administration.

electromagnets, and $\{\bar{T}_d\}$ represents external disturbance torques. A bar over a variable indicates that it is referenced to core coordinates. The translational acceleration of the core, in core coordinates, can be written as

$$\{\ddot{\bar{r}}\} = (1/m_c) \left(\text{Vol} \left([T_m][\partial B][T_m]^{-1}\{\bar{M}\} \right) + \{\bar{F}_d\} \right) \quad (2)$$

where m_c is the mass of the core, $[\partial B]$ is a matrix of the gradients of B , and $\{\bar{F}_d\}$ represents external disturbance forces in core coordinates. Under the assumptions of reference 1, $\{B\}$ can be written as

$$\{B\} = (1/I_{\max}) [K_B]\{I\} \quad (3)$$

where I_{\max} is the maximum coil current, $[K_B]$ is a 3×5 matrix whose elements represent the values of $\{B\}$ produced by a corresponding coil driven by the maximum current and the coil currents are

$$\{I\}^T = [I_1 \ I_2 \ I_3 \ I_4 \ I_5] \quad (4)$$

The gradients can be put in the same form by arranging the elements of $[\partial B]$ as a column vector. This results in

$$\{\partial B\} = (1/I_{\max}) [K_{\partial B}]\{I\} \quad (5)$$

where $\{\partial B\}$ is a nine element column vector containing the gradients of $\{B\}$, and $[K_{\partial B}]$ is a 9×5 matrix whose elements represent the values of $\{\partial B\}$ produced by a corresponding coil driven by the maximum current. The simplified notation from reference 1, where B_{ij} represents $\partial B_i/\partial j$, will be used for gradients. Each element of $\{\partial B\}$, for example B_{xx} , can be written in the form

$$B_{xx} = (1/I_{\max}) [K_{xx}]\{I\} \quad (6)$$

where $[K_{xx}]$ is a 1×5 matrix containing values of B_{xx} produced by a corresponding coil driven by the maximum current. A block diagram of the system is shown in figure 2. This model is nonlinear because of the coordinate transformations and is of the form

$$\dot{x} = f(x, u) \quad (7)$$

where x is given by

$$x^T = [\bar{\Omega}_y \ \bar{\Omega}_z \ \bar{V}_x \ \bar{V}_y \ \bar{V}_z \ \theta_y \ \theta_z \ x \ y \ z] \quad (8)$$

and the input u is given by

$$u^T = [I_1 \ I_2 \ I_3 \ I_4 \ I_5] \quad (9)$$

The states θ_y and θ_z in (8) are the pitch and yaw angles of the core respectively. Analyses and simulations of the model were performed using MATRIX_X with SYSTEM_BUILD. A description of the MATRIX_X/SYSTEM_BUILD implementation is presented in Appendix B. LGMSS model parameters are presented in Table A1.

CONTROLLER DESIGN APPROACH

The control approach which was investigated was to linearize the system about a nominal operating point x_o, u_o and then use the resulting linear model to calculate feedback gains to stabilize and control the core about this point. The equations for computing u_o for a given x_o are presented in the appendix of reference 1. The feedback gains for the linearized system were calculated using LQR theory. In this approach the system is put in state variable form

$$\dot{x} = Ax + Bu \quad (10)$$

and a set of full state feedback gains are calculated that minimizes the quadratic cost function

$$J = \int_0^{\infty} (x^T Q x + u^T R u) dt \quad (11)$$

where the weighting matrices, Q and R , are symmetric and positive-semidefinite and positive-definite, respectively. The resulting control law is

$$u = -K_R x \quad (12)$$

where

$$K_R = R^{-1} B^T P \quad (13)$$

and P is a symmetric positive-definite matrix satisfying the matrix Riccati equation (see ref. 2)

$$PA + A^T P + Q - PBR^{-1}B^T P = 0 \quad (14)$$

The operation of the LGMSS requires that the control system provide variable set point control and also that it compensate for a constant disturbance (the weight of the core). Two feedback controller configurations which meet these requirements were investigated and are described below.

Nonzero set point regulator with constant disturbance.- With a constant disturbance, V_o , the system under consideration becomes

$$\dot{x} = Ax + Bu + V_o \quad (15)$$

The controlled variables are assumed to be

$$z = Dx \quad (16)$$

For the LGMSS, z is defined as

$$z^T = [\theta_y \ \theta_z \ x \ y \ z] \quad (17)$$

For a set point of z_o , a constant input u_o must be found to hold the states at x_o so that

$$z_o = Dx_o \quad (18)$$

From (15) above, x_o and u_o must be related by

$$0 = Ax_o + Bu_o + V_o \quad (19)$$

Next, define the shifted input, shifted state, and shifted controlled variable, respectively, as

$$u' = u - u_o \quad (20)$$

$$x' = x - x_o \quad (21)$$

$$z' = z - z_o \quad (22)$$

Solving equations (20)–(22) for u , x , and z , substituting the results into (15) and (16) and using (18) and (19), it can be shown that the shifted variables satisfy the equations

$$\dot{x}' = Ax' + Bu' + V_o \quad (23)$$

and

$$z' = Dx' \quad (24)$$

Assume the shifted regulator problem has a steady-state solution in the form of the control law

$$u' = -Fx' \quad (25)$$

that minimizes the quadratic cost function

$$J = \int_0^{\infty} (x'^T Q x' + u'^T R u') dt \quad (26)$$

where F is a matrix of constant feedback gains. From (25) and (20)-(22)

$$u = -Fx + u_o + Fx_o \quad (27)$$

which has the form

$$u = -Fx + u'_o \quad (28)$$

where the constant vector u'_o is to be determined so that in steady-state the controlled variable z assumes the given value z_o . Substituting (28) into (15) gives

$$\dot{x} = (A - BF)x + Bu'_o + V_o \quad (29)$$

Since the closed-loop system is assumed stable, as $t \rightarrow \infty$ the states approach x_o which satisfies

$$0 = \bar{A}x_o + Bu'_o + V_o \quad (30)$$

where

$$\bar{A} = A - BF \quad (31)$$

For a stable system \bar{A} is nonsingular and x_o becomes

$$x_o = (-\bar{A})^{-1}Bu'_o + (-\bar{A})^{-1}V_o \quad (32)$$

z_o then becomes

$$z_o = D(-\bar{A})^{-1}Bu'_o + D(-\bar{A})^{-1}V_o \quad (33)$$

and solving for u'_o results in

$$u'_o = [D(-\bar{A})^{-1}B]^{-1}z_o - [D(-\bar{A})^{-1}B]^{-1}D(-\bar{A})^{-1}V_o \quad (34)$$

A block diagram of this controller is shown in figure 3.

Integral feedback regulator.- Another controller configuration which was investigated is one which uses integral feedback. Integral feedback is often used in systems subjected to constant disturbances in order to minimize steady-state errors (ref. 2). To develop the integral feedback controller equations, assume the system of (15) with the controlled variables defined by (16). To the system of (15) add the integral states q , defined by

$$\dot{q} = z' \quad (35)$$

where z' is defined by (22). A performance function can now be defined as

$$J = \int_0^{\infty} (z^T \bar{Q}z + q^T Qq + u^T Ru) dt \quad (36)$$

Assume that the time-invariant control law

$$u = -F_1x - F_2q \quad (37)$$

can be found which stabilizes the augmented system described by (15), (16), and (35), and which minimizes (36). Since the presence of the constant disturbance vector in (15) has no effect on the asymptotic stability of the system

$$\lim_{t \rightarrow \infty} \dot{q} = 0 \quad (38)$$

and from (35)

$$\lim_{t \rightarrow \infty} z' = 0 \quad (39)$$

This means that the control system with the control law (37) has the property that the error in the controlled variables, due to a constant input disturbance, eventually goes to zero. A block diagram of the integral feedback regulator is shown in figure 4.

Initial conditions.- The initial conditions on current for the nonzero set point regulator with a given x_o and z_o can be determined from equation (34). The initial conditions on the integrator outputs, for the integral feedback regulator, can be determined from (15) and (37). In equilibrium, assuming a stable system, (15) reduces to (19). Substituting (37) into (19) results in

$$0 = \bar{A}x_o - BF_2q_o + V_o \quad (40)$$

where $\bar{A} = A - BF_1$. Solving for x_o results in

$$x_o = \bar{A}^{-1}BF_2q_o - \bar{A}^{-1}V_o \quad (41)$$

and z_o becomes

$$z_o = D\bar{A}^{-1}BF_2q_o - D\bar{A}^{-1}V_o \quad (42)$$

Finally, q_o becomes

$$q_o = \left(D\bar{A}^{-1}BF_2\right)^{-1} z_o + \left(D\bar{A}^{-1}BF_2\right)^{-1} D\bar{A}^{-1}V_o \quad (43)$$

Discrete model.- The equations presented above are for a continuous system and assume a perfect sensor with zero delay. In order to investigate the effects of a delay introduced by a finite sensor processing time, a worst case sampling time of 20 samples per second was assumed. The continuous system equations were discretized and discrete system gains were calculated using this sample time. The sensor delay time was modeled as a zero order hold (ZOH) on the output of the nonlinear open-loop system for simulation purposes. A block diagram showing the placement of the ZOH for the integral feedback regulator is shown in figure 5.

ANALYSIS AND SIMULATION RESULTS AND DISCUSSION

This section presents the analysis and simulation results for the nonzero setpoint and integral feedback regulator which were obtained by using the MATRIX_X implementation described in Appendix B. The results are for positioning accuracy of the the two approaches, with fixed gains, over large angular displacements about the yaw axis. The approach was to define, first of all, the range over which a set of fixed gains was stable for each regulator type. This was accomplished by obtaining linearized models of the open-loop system at intervals of two degrees yaw. Feedback gains were computed for a given reference angle and these gains were then used with the linearized models to obtain closed-loop eigenvalues over a given range of yaw angles approaching the limits of stability. The full nonlinear model was then simulated using feedback gains calculated at a given yaw angle. Inputs to the system consisted of position commands in one degree increments. For more detail on the design model used, see Appendix B.

Continuous System

Nonzero set point regulator.- A plot of the eigenvalues of the nonzero set point regulator with feedback gains calculated for the model linearized around zero yaw angle, as the core is rotated through increments of two degrees, is shown in figure 6. The low frequency eigenvalues are shown on an expanded scale in figure 7. The point at which the eigenvalues cross over the imaginary axis is at a yaw angle of approximately 42 degrees. A plot of the eigenvalues, with the same feedback gains, as the model is rotated from zero degrees to -42 degrees is shown in figure 8. The low frequency eigenvalues are shown on an expanded scale in figure 9. As expected, because of symmetry, these eigenvalue plots are identical with the previous plots. Further calculations also verified that this pattern repeats every 36 degrees. That

is, fixed gains calculated at zero, 36, 72, ect. are stable over a range of plus and minus 42 degrees around the angle for which the gains are calculated. The system performance was evaluated by commanding yaw position over a range of 18 degrees in increments of one degree. Time between increments was 20 seconds. Figure 10 is a plot of the input command and figure 11 is a plot of the actual yaw angle. Figure 12 is a plot of the difference between command and actual angle. Figures 13 through 16 show the response of the pitch, x , y , and z axes. As can be seen, the errors build up as the yaw angle increases. This is the main disadvantage of the nonzero set point controller for this particular application. The input which minimizes the position error for a given command and constant input disturbance is given by equation (34) and is a function of \bar{A} which is in turn a function of A . As evident from the block diagram of the analytical model in figure 2, A is a function of core position. The system response to a command over a negative 18-degree range was essentially the same and is not shown. The system response about other nominal gain points, at 36-degree intervals in yaw, was also essentially the same.

Integral feedback regulator.- A plot of the eigenvalues for the integral feedback regulator with fixed gains calculated for the model linearized around zero yaw angle is shown in figure 17. The low frequency eigenvalues are shown on an expanded scale in figure 18. The symmetry properties for the nonzero set point regulator discussed above were found to apply to the integral feedback regulator also. The response of the system with the integral feedback controller with fixed gains calculated at zero degrees, to the command input shown in figure 19, is shown in figure 20. The yaw error is shown in figure 21 and the response of the pitch, x , y , and z axes are shown in figures 22 through 25. As can be seen from these figures, and as predicted by equation (39), after an initial transient the errors all go to zero. As was the case with the nonzero set point regulator discussed above, system response about other nominal gain points (at 36-degree intervals in yaw) was essentially the same.

Discrete System

Integral feedback regulator.- After evaluating the performance of the nonzero set point regulator with a continuous system model, a decision was made to drop this approach from further consideration and concentrate on the integral feedback regulator for the discrete system evaluation. A plot of the eigenvalues of the discrete integral feedback regulator with feedback gains calculated for the model linearized around zero yaw angle, as the core is rotated through increments of two degrees, is shown in figure 26. The eigenvalues shown have been mapped from the z -plane into the s -plane. The low frequency eigenvalues are shown on an expanded scale in figure 27. As can be seen from the figures, the range of stable operation is reduced from 42 degrees for the continuous system to approximately 36 degrees for the discrete system. The discrete system was symmetric about points 36 degrees apart in yaw angle as was the continuous system. The response of the discrete integral feedback controller with fixed gains, calculated for the model linearized around zero degrees, to the command input shown in figure 28 is shown in figure 29. The yaw error is shown in figure 30 and the response of the pitch, x , y , and z axes are shown in figures 31 through 34. The transients in the response of the discrete system were of higher magnitude than the continuous system but not by a significant amount. Other than magnitudes, the responses were similar with the errors returning to zero after initial transients.

CONCLUDING REMARKS

Two control approaches for a Large Gap Magnetic Suspension System (LGMSS) have been investigated and numerical results presented. The control approaches investigated were a nonzero set point regulator with constant disturbance input and an integral feedback regulator. The LGMSS provides five degrees of freedom control of a suspended element which is a cylinder composed of permanent magnet material. The magnetic actuators are air core electromagnets mounted in a planar array. Results were obtained for both continuous system and discrete system models. The continuous system model assumed a perfect position sensor with no delays and the discrete system model assumed a worst case delay introduced by the sensor of fifty milliseconds. All analyses and simulations were performed using MATRIX_X with System_BUILD. The numerical results are for positioning accuracy, with fixed gains, over large angular

displacements about the yaw axis. These results indicate that for the LGMSS investigated, the integral feedback regulator provides the best performance. Also, for control of yaw over a range of 360 degrees, scheduled gains will be required. Based on the numerical results, control about a nominal operating point is possible over a range of plus or minus 18 degrees. Although the system is stable over a greater range, transient errors become larger as the yaw angle is increased and plus or minus 18 degrees appears to be a reasonable limit. Gains can be scheduled over a smaller interval based on particular requirements. Control of pitch over large angles was not addressed in this investigation and should be the subject of a future effort.

The results presented in this paper, for the analytical model utilized, indicate that delays introduced by the position sensor, for the worst case value investigated, can be adequately compensated. Future efforts should include investigations of the effects on performance of: 1) different output feedback approaches, 2) changes in $\{B\}$ and $[\partial B]$ with core displacement, 3) power supply and coil dynamics, and 4) sensor hardware characteristics.

APPENDIX A

CALCULATION OF ELECTROMAGNET FIELDS AND GRADIENTS

By

Colin P. Britcher
 Department of Mechanical Engineering and Mechanics
 Old Dominion University
 Norfolk, Virginia

Magnetic fields external to air-cored electromagnets of simple geometry can be calculated accurately by the use of line conductor models. A computer program FORCE (ref. 5) represents such electromagnets by an assembly of straight line conductor elements. Fields and field gradients produced by each element at any point, not coincident with the element, may then be calculated exactly using the Biot Savart law. Fields and field gradient components are then simply summed over all conductor elements. This approach is illustrated in figure A1.

This procedure is accurate if the number of conductor elements is large enough to properly represent the three-dimensionality of the electromagnet yet small enough to avoid excessive accumulation of numerical (rounding) errors. Accuracy generally improves with distance from the electromagnet as the effects of the discontinuous representation of current are reduced. Recalculation with greater or lesser numbers of elements is a straightforward and effective check on the reliability of the solution.

Calculations using FORCE were made for the electromagnet configuration used in the earlier stages of the design study reported in reference 6. The parameters for this system are summarized in table A1 and a schematic representation is given in figure A2. Calculation results are presented in table A2. It should be noted that detail adjustments to the configuration and to the design suspension height were made later in the design study mentioned above but do not substantially affect the results shown here or the conclusions of this report.

TABLE A1.- LGMSS MODEL PARAMETERS

Core diameter, m	0.1016
Core length, m	0.3048
Core mass (m_c), kg	22.76
Core inertia (I_c), kg-m ²	0.6
Core volume (Vol), m ³	$2.5(10)^{-3}$
Core magnetization (M_r), A/m	$9.5493(10)^5$
Core suspension height (h), m	0.9144
Electromagnet outer radius, m	0.386
Electromagnet inner radius, m	0.173
Electromagnet height, m	0.493
Maximum electromagnet current (I_{max}), A	559.5

TABLE A2. - ELECTROMAGNET FIELDS AND GRADIENTS

Electromagnet	B_X	B_Y	B_Z	B_{XX}	B_{XY}	B_{XZ}	B_{YY}	B_{YZ}	B_{ZZ}
	(Tesla)			(Tesla/meter)					
1	-.0237	0	+.0218	-.0101	0	+.0544	+.0338	0	-.0237
2	-.0073	-.0225	+.0218	+.0296	-.0129	+.0168	-.0059	+.0518	-.0237
3	+.0192	-.0139	+.0218	+.0051	+.0209	-.0440	+.0186	+.0320	-.0237
4	+.0192	+.0139	+.0218	+.0051	-.0209	-.0440	+.0186	-.0320	-.0237
5	-.0073	+.0225	+.0218	+.0296	+.0129	+.0168	-.0059	-.0518	-.0237

Fields correspond to maximum rated current for each electromagnet (559.5 Amp.).

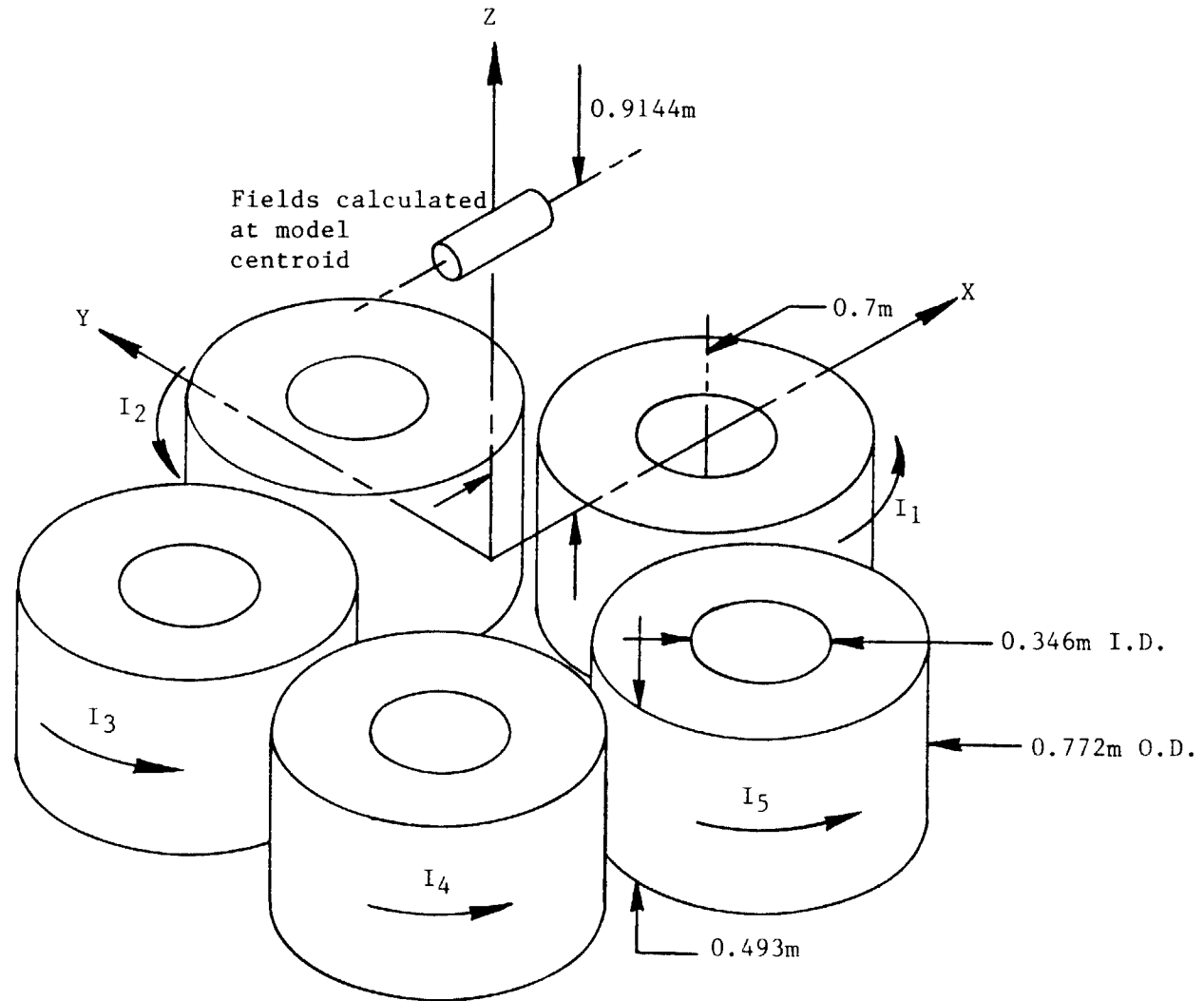


Figure A1.-Geometry used for magnetic field calculations.

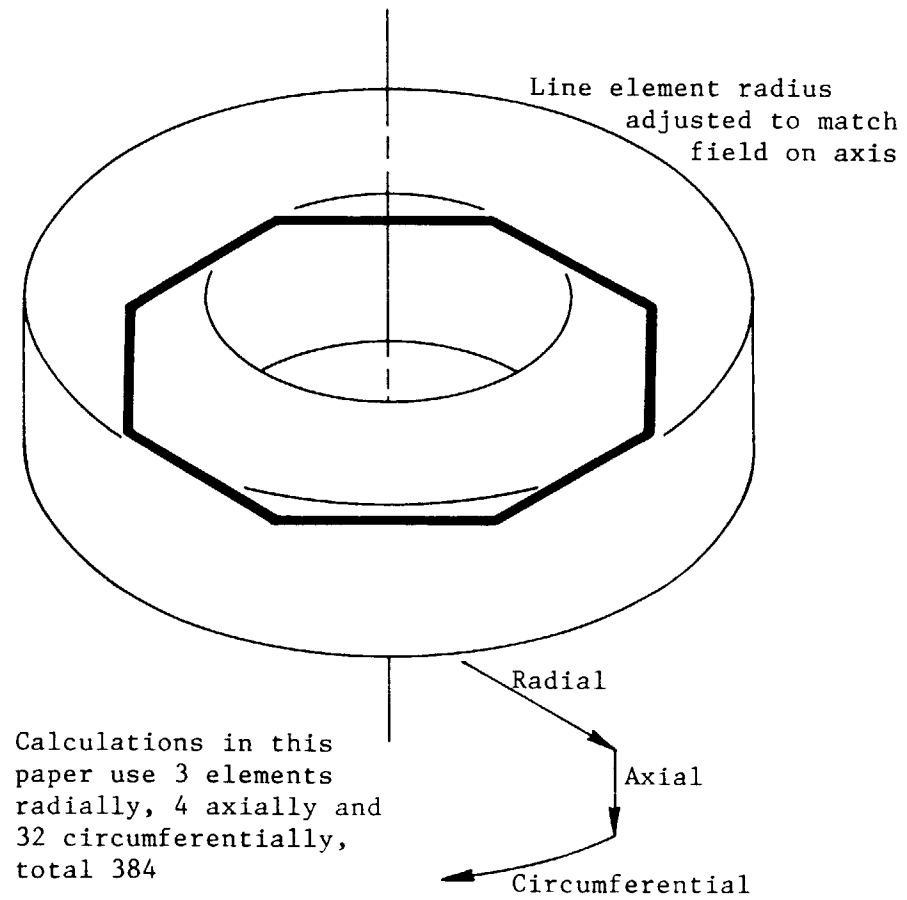


Figure A2.-Representation of electromagnets by line conductor elements.

APPENDIX B

MATRIX_X IMPLEMENTATION

The process of implementing the LGMSS plant model and control approaches, using MATRIX_X and SYSTEM_BUILD, involves the construction of block diagram representations of the system (figure B1) and the controllers (figures B2, B3, and B4). Since version 6.0 of MATRIX_X/SYSTEM_BUILD was used to construct the models, it was necessary to break the implementation into nested super blocks containing a maximum of 6 blocks each (for more detailed information on MATRIX_X/SYSTEM_BUILD see refs. 3 and 4). Figure B5 shows the actual super blocks of the implementation. Each of the blocks in figure B1 can be identified as a block within some level of the nested super blocks shown in figure B5. For the sake of brevity and clarity only the unnested versions of the SYSTEM_BUILD models will be shown and discussed from this point on.

There is a correspondence between blocks in the block diagram of the system (figure 2) and blocks, or groups of blocks, in the SYSTEM_BUILD implementation of figure B1. For instance, the leftmost block in figure 2 is modeled by the super block labeled FIELDS in figure B1. The expression $(1/I_{\max})$ is represented by the gain block labeled I MAX in which each of the 5 outputs is calculated by multiplying the corresponding input by a constant gain factor of $(1/I_{\max})$. The K matrix multiplication is implemented by the State Space block labeled XYZ which multiplies the vector of 5 currents by a 5×12 matrix to calculate the vector of 12 outputs corresponding to the 3 field components (B_x, B_y, B_z) and the 9 gradients $(B_{xx}, B_{xy}, B_{xz}, B_{yx}, B_{yy}, B_{yz}, B_{zx}, B_{zy}, B_{zz})$.

One block found in figures B1 and B5 has no corresponding element in the system block diagram of figure 2. This block, labeled A GRAV outputs a vector $[0 \ 0 \ g]$ which is passed through a transformation from inertial to body coordinates (block TM) and summed with the linear accelerations to model the effects of gravity on the core.

In order to set up for calculation of the LQR gains, the SYSTEM_BUILD ANALYZE option is invoked on the super block OPEN (fig. B6). This super block contains a super block labeled PLANT, which is the highest level super block in the plant model of figure B5 (and represents the whole of fig. B1). Super block OPEN also has a step input block labeled I OFF which sets the initial currents about which the nonlinear system will be linearized and a gain block labeled CONTIN. The CONTIN block has unity gain and acts as a place holder for a zero order hold super block used in discrete versions of the system as will be discussed below. The yaw angle (θ_z) for linearization is established by setting initial conditions on the corresponding integrator prior to analysis of the model.

The ANALYZE operation returns from the SYSTEM_BUILD module to MATRIX_X where the LINearize function is invoked to calculate the linearized state space representation of the nonlinear system represented by PLANT. LIN returns an S matrix and NS , the number of states in S (10 for this model). The state space matrix S can be partitioned into

$$S = \left[\begin{array}{c|c} A & B \\ \hline C & \bar{D} \end{array} \right] \quad (\text{B1})$$

where A and B are the matrices in the state variable representation of the system in equation 10. The matrix A will be of dimension $NS \times NS$, B will be dimensioned $NS \times NI$, C will be $NO \times NS$ and \bar{D} will be $NO \times NI$; where NI is the number of inputs (5 currents) and NO is the number of outputs ((X, Y, Z) positions and velocities, Y and Z rotation angles and rotational velocities). The MATRIX_X function SPLIT(S, NS) accomplishes this partitioning and can return A and B only or all four matrices. For the problem being considered only A and B are of interest since C turns out to be an identity matrix

and D is a zero matrix. The output equation

$$y = Cx + Du \quad (B2)$$

reduces to

$$y = x \quad (B3)$$

since the outputs are the position and velocity variables corresponding to the states, and outputs are not directly related to inputs. For the model linearized around zero, the A matrix becomes

$$A = \left[\begin{array}{c|ccccc} & 162.17 & 0 & 0 & 0 & 0 \\ 5 \times 5 & 0 & 162.17 & 0 & 0 & 0 \\ [0] & -9.8066 & 0 & 0 & 0 & 0 \\ & 0 & 0 & 0 & 0 & 0 \\ & -0.0147 & -0.0049 & 0 & 0 & 0 \\ \hline 5 \times 5 & & & & & 5 \times 5 \\ [I] & & & & & [0] \end{array} \right] \quad (B4)$$

and the B matrix becomes

$$B = \left[\begin{array}{ccccc} -0.155 & -0.155 & -0.155 & -0.155 & -0.155 \\ 0 & -0.16 & -0.098 & 0.098 & 0.16 \\ -0.0019 & 0.0055 & 0.001 & 0.001 & 0.0055 \\ 0 & -0.0024 & 0.0039 & -0.0039 & 0.0024 \\ 0.102 & 0.0031 & -0.0082 & 0.0082 & 0.0031 \\ \hline & & & & 5 \times 5 \\ & & & & [0] \end{array} \right] \quad (B5)$$

This model has four nonzero eigenvalues: -12.7346 , -12.7346 , 12.7346 , and 12.7346 .

A SYSTEM_BUILD implementation of the linearized model was constructed for use in testing and is shown in figure B7. The full nonlinear model was employed for all simulations shown in this document.

The nonzero set point regulator gains can then be calculated using the linearized model represented by A and B , and the Q and R matrices from the quadratic cost function of equation 26. The Q and R matrices used for gain calculation were

$$Q = [1(10)^6] \quad (B6)$$

and

$$R = [I] \quad (B7)$$

where Q is a 10×10 diagonal matrix and R is a 5×5 identity matrix. The MATRIX_X function REGULATOR calculates the LQR gain matrix F and the corresponding eigenvalues, EV . As a baseline, the closed-loop eigenvalues for the system with the model linearized around zero and gains calculated using (B6) and (B7) are presented in figures B8 and B9. The nonzero set point matrix HCI can then be calculated. HCI is given by

$$HCI = [D(-\bar{A})^{-1}B]^{-1} \quad (B8)$$

where D is defined in equation 16. For this implementation the only nonzero elements in D are those corresponding to X , Y , Z , θ_y , and θ_z . The value of each nonzero element is one. The SYSTEM_BUILD

implementation of the nonzero set point controller is shown in figure B2 and corresponds to the conventional block diagram of figure 3. Currents as well as position and rotation variables are brought to the output. Inputs and outputs are scaled to appear in inches and degrees while internal quantities are meters and radians.

The integral feedback continuous LQR gains were calculated similarly by augmenting the linear state space model, represented by A and B , with 5 new states corresponding to the feedback integrators:

$$A' = \left[\begin{array}{cc|c} 10 \times 10 & & 5 \times 5 \\ [A] & & [0] \\ \hline 5 \times 5 & 5 \times 5 & 5 \times 5 \\ [0] & [I] & [0] \end{array} \right] \quad (B9)$$

$$B' = \left[\begin{array}{c} 10 \times 5 \\ [B] \\ \hline 5 \times 5 \\ [0] \end{array} \right] \quad (B10)$$

The $MATRIX_X$ function $REGULATOR$ was again used to calculate LQR gains. The closed-loop eigenvalues for the integral feedback system with the model linearized around zero and gains calculated using (B6), extended to a 15×15 diagonal matrix, and (B7) are presented in figures B10 and B11. Figure B3 shows the $SYSTEM_BUILD$ model of the continuous integral feedback controller of figure 4. The delay due to the sensor was modeled by using the $MATRIX_X$ $DISCRETIZE$ function which takes as parameters a state space matrix, S , its order, NS , and a delay TAU which was specified as 0.05 seconds, and returns a discrete state space matrix SD . A state space matrix for the augmented system, S' , was constructed using A' and B' above as well as dummy C' and D' . The discretized version of this matrix, SD , is then $SPLIT$ and the resulting AD and BD system matrices used with $MATRIX_X$ function $DREGULATOR$, similar to $REGULATOR$ discussed above, to calculate LQR feedback gains for the discrete version of the system. The closed-loop eigenvalues for the discrete system with the model linearized around zero and gains calculated using (B6), extended to a 15×15 diagonal matrix, and (B7) are presented in figures B12 and B13. The eigenvalues shown have been mapped from the z -plane into the s -plane. Figure B14 shows the $SYSTEM_BUILD$ model of the discrete integral feedback controller of figure 5. The discrete super block ZOH is the sensor model. It replaces the $CONTIN$ block and acts as a Zero Order Hold. ZOH is the only discrete super block used in this otherwise continuous model.

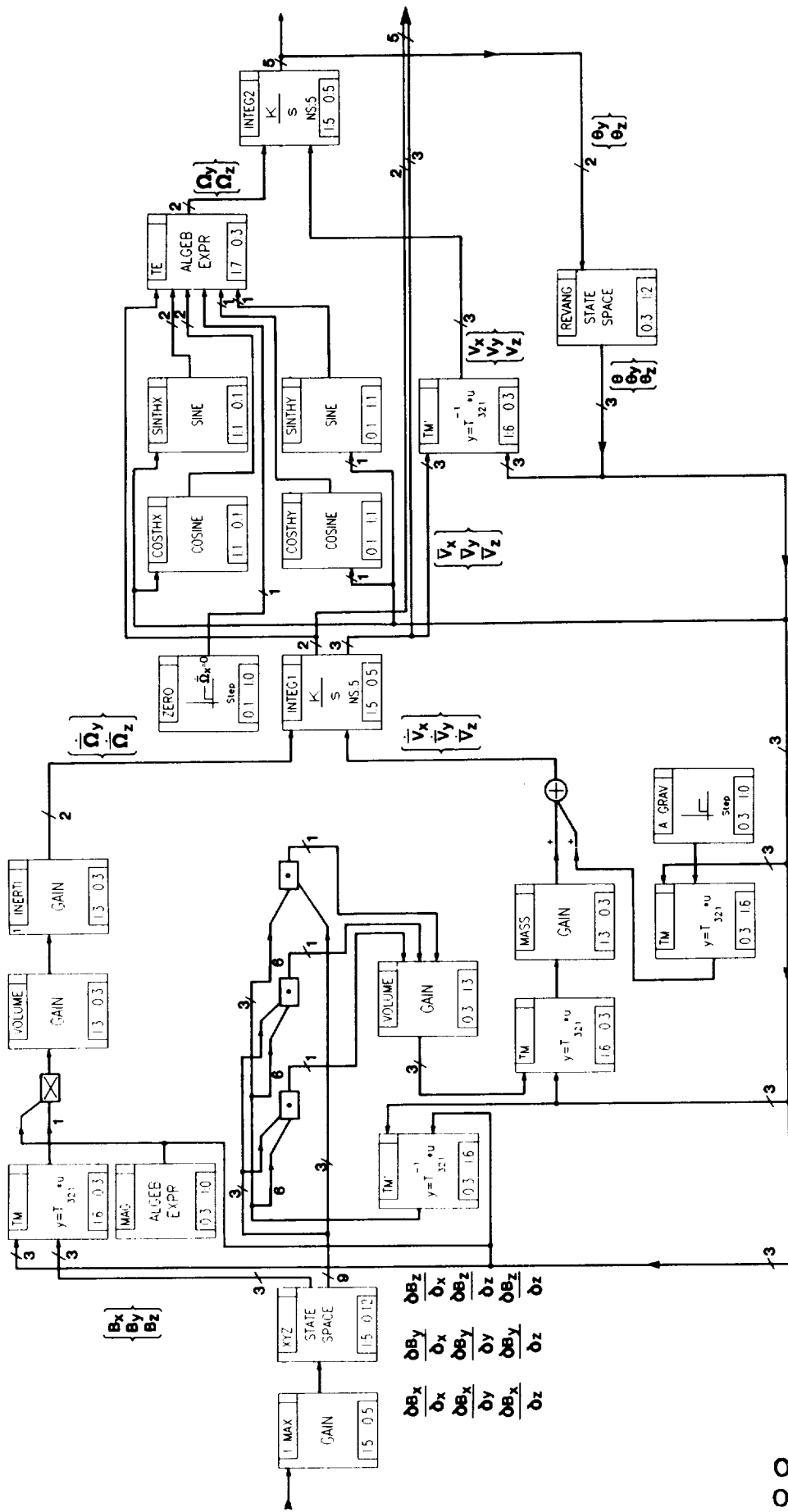


Figure B1 .-Nonlinear open-loop system.

ORIGINAL PAGE IS OF POOR QUALITY

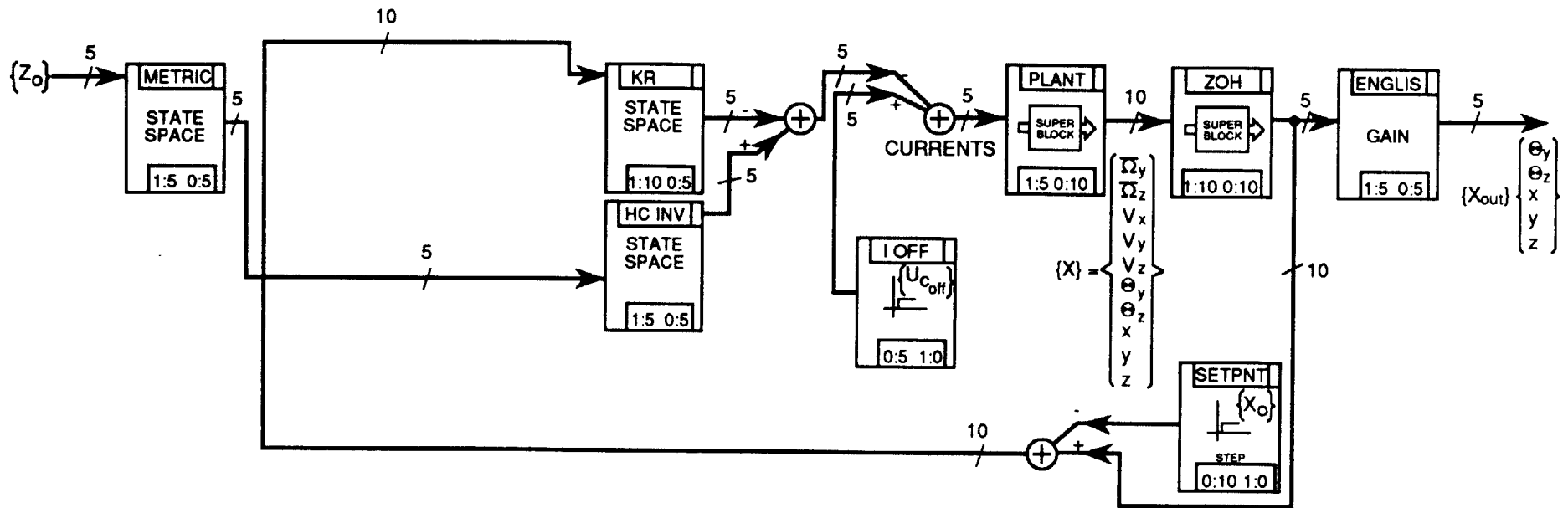


Figure B2.-Nonzero set point regulator.

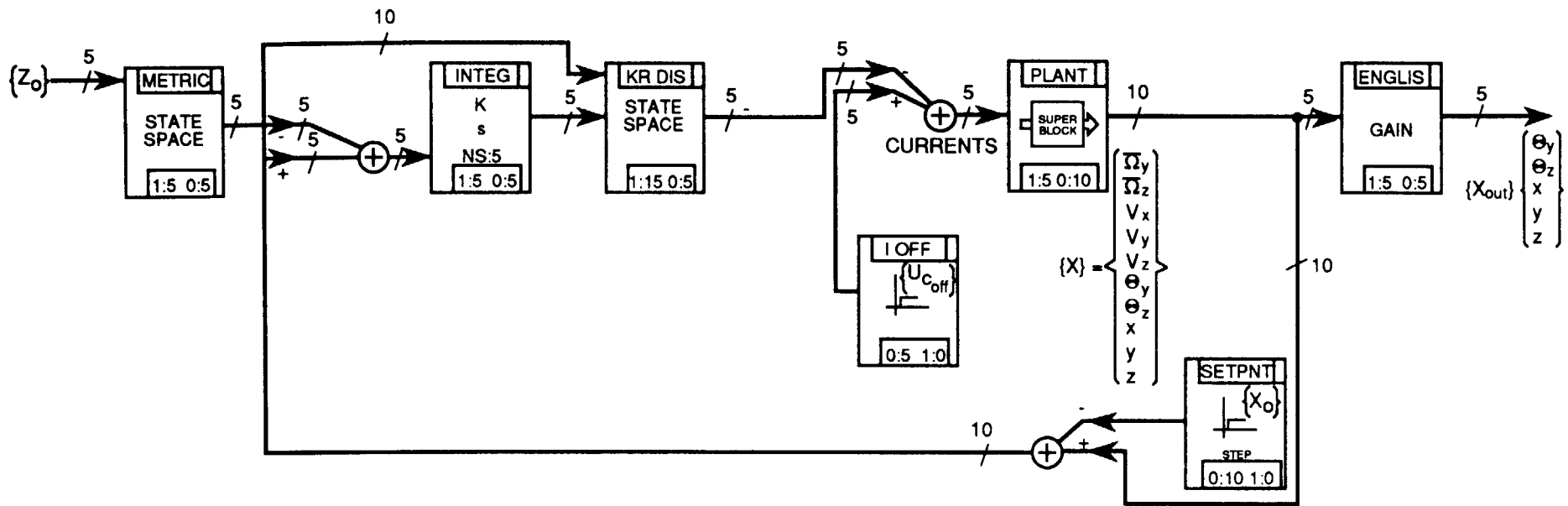


Figure B3.-Integral feedback regulator.

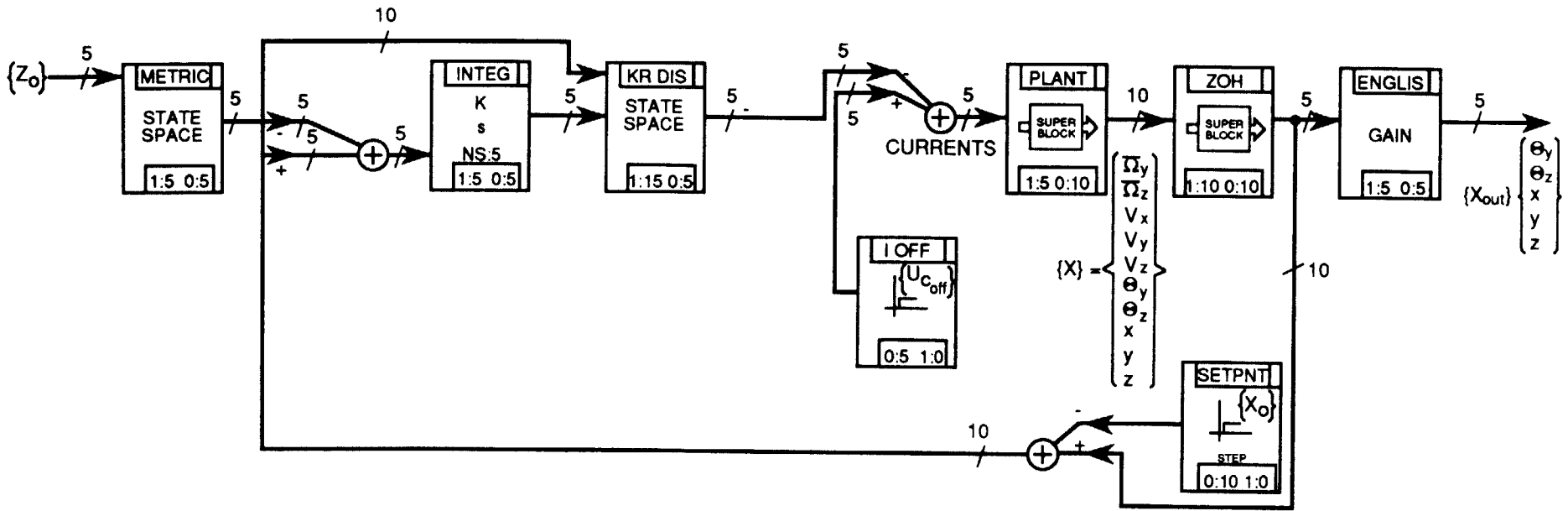


Figure B4.-Integral feedback regulator with zero order hold.

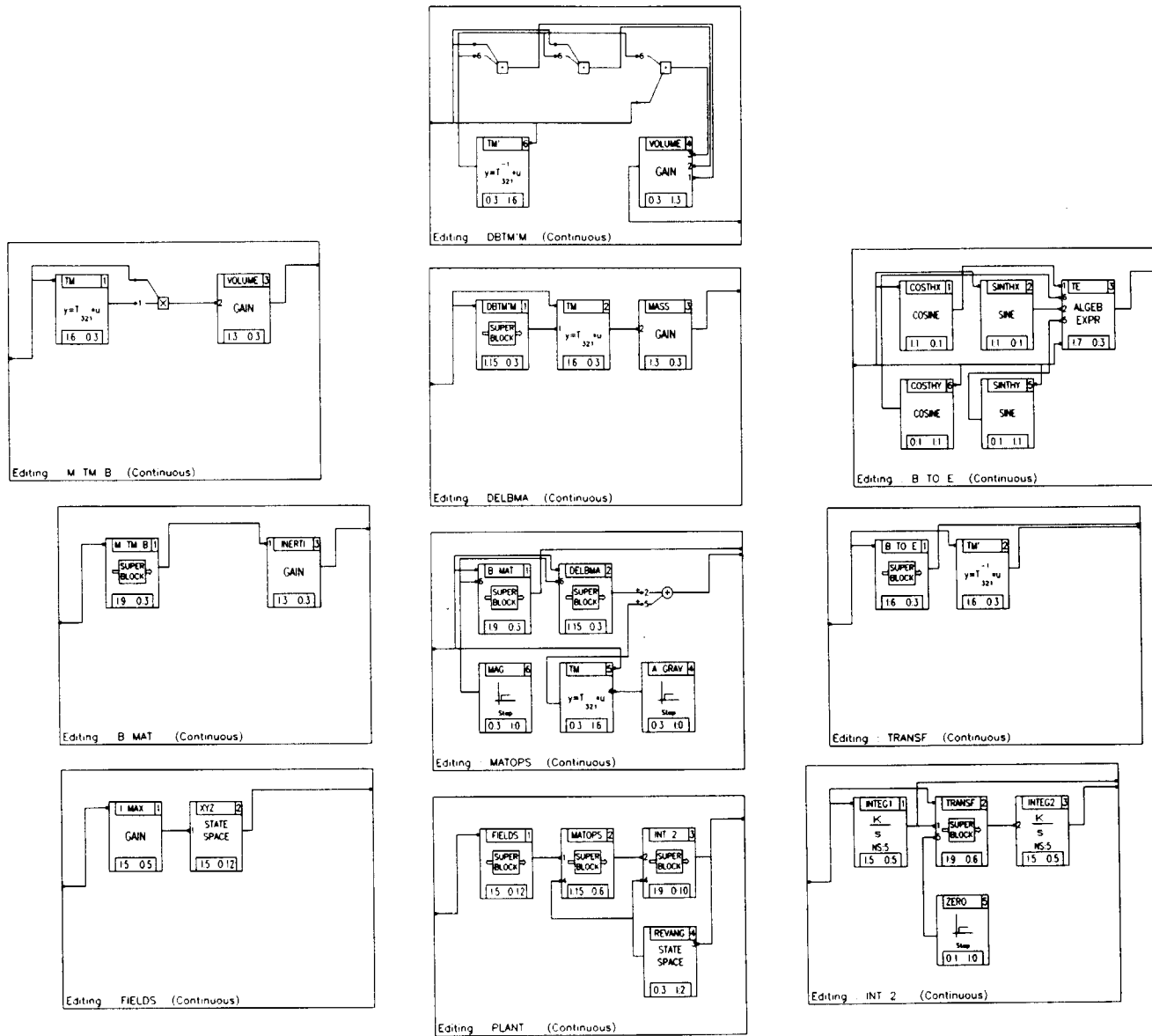


Figure B5.-Nested super block model of nonlinear open-loop system.

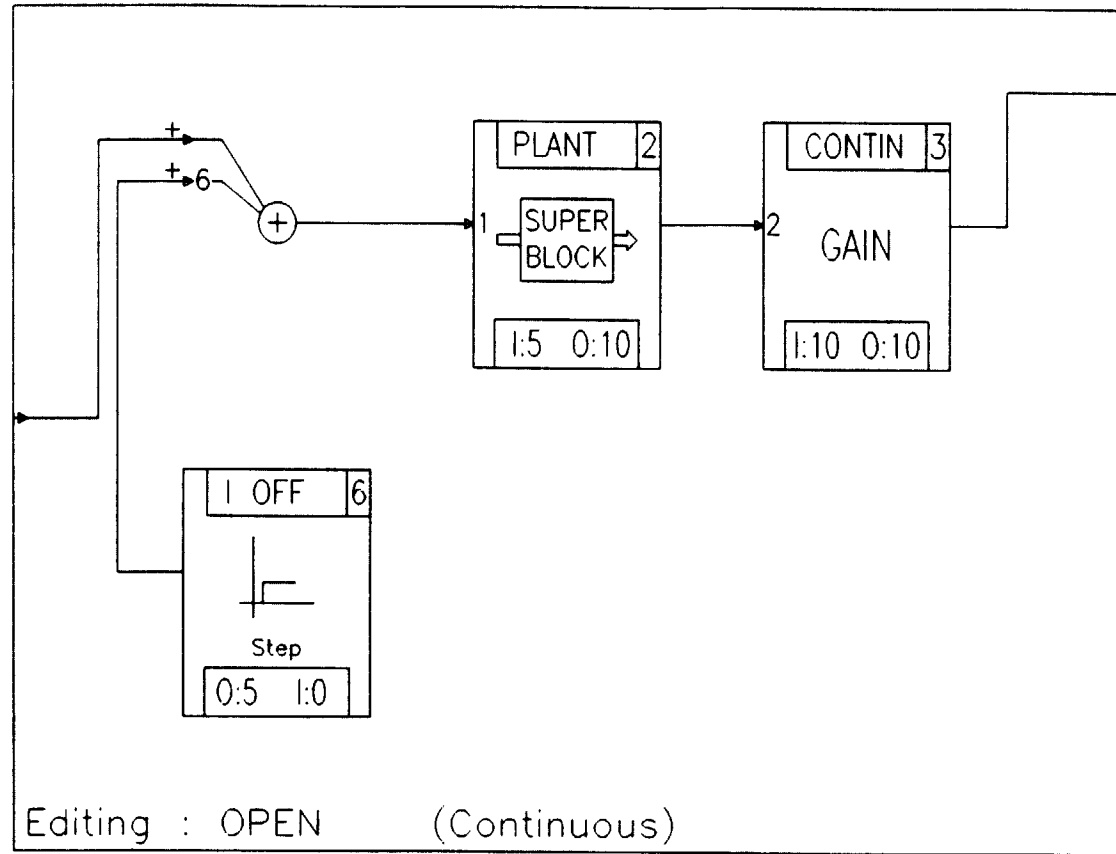


Figure B6.-Open-loop system used for linearization.

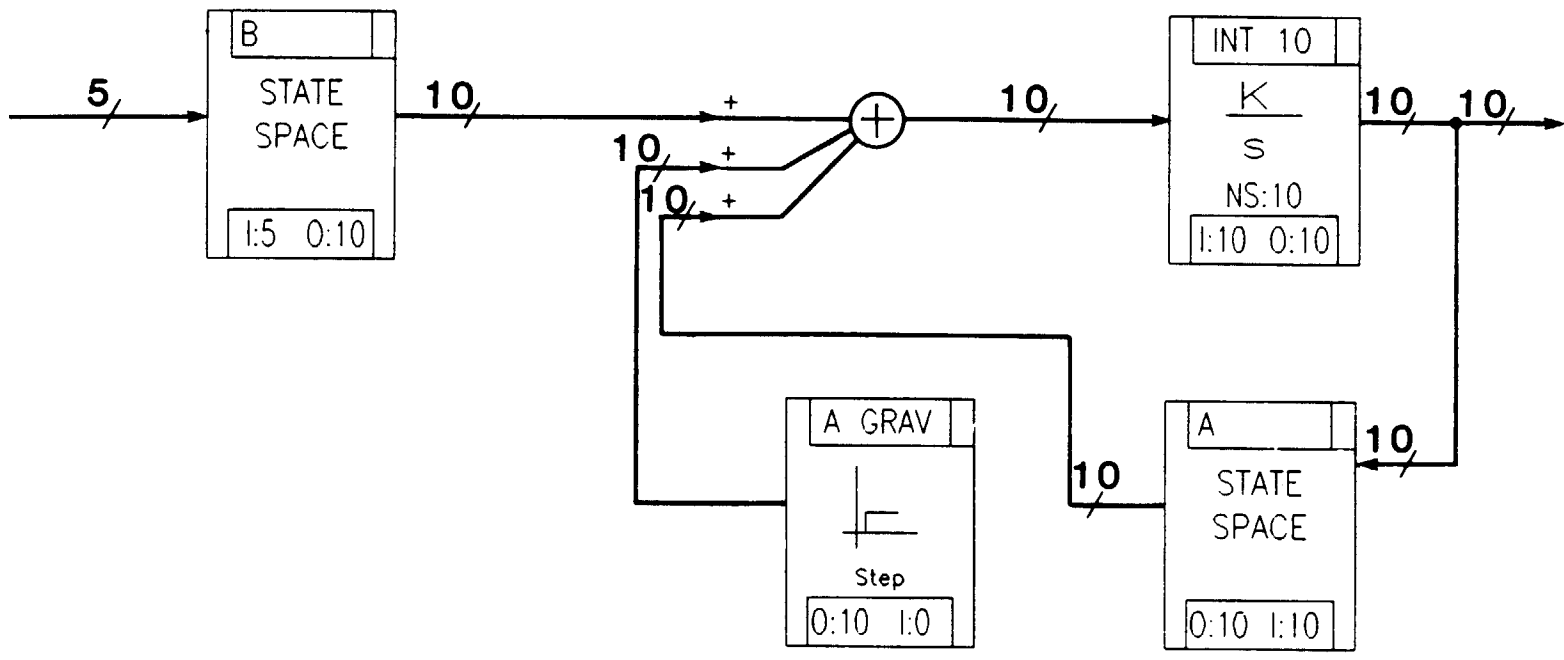


Figure B7.-Linearized open-loop system.

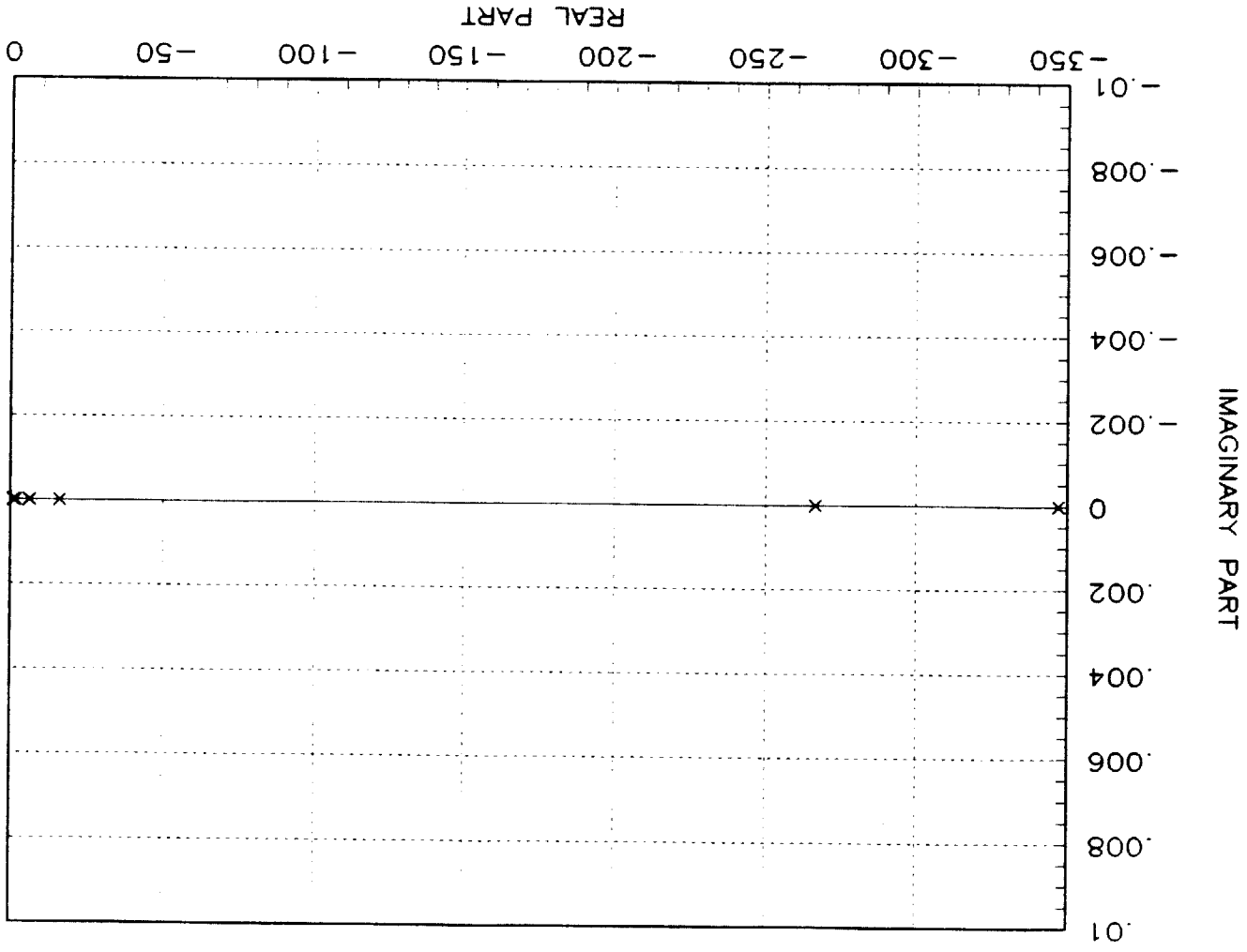


Figure B8.-Closed-loop eigenvalues of the system with the model linearized around zero.

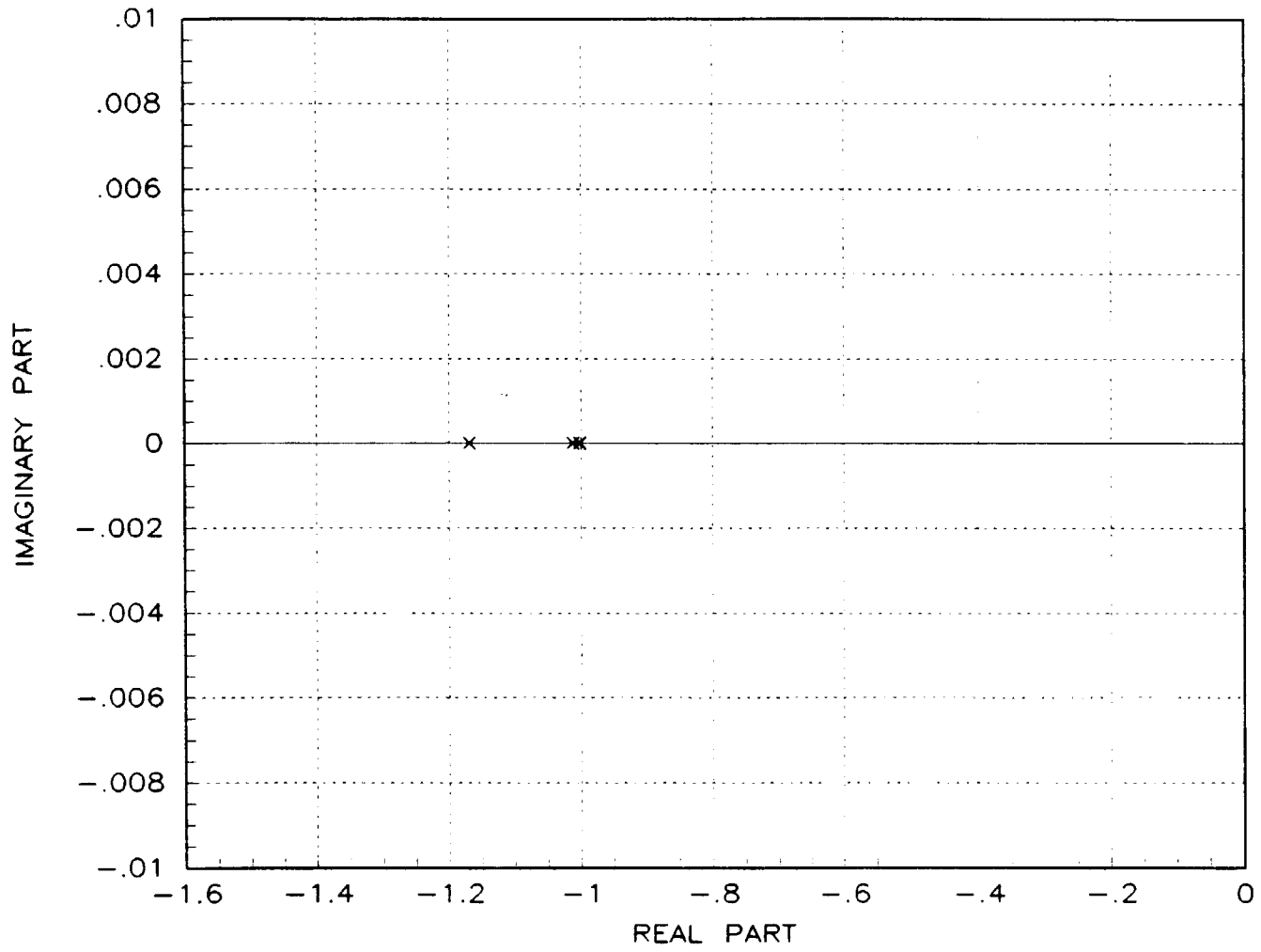


Figure B9.- Low frequency eigenvalues of figure B8.

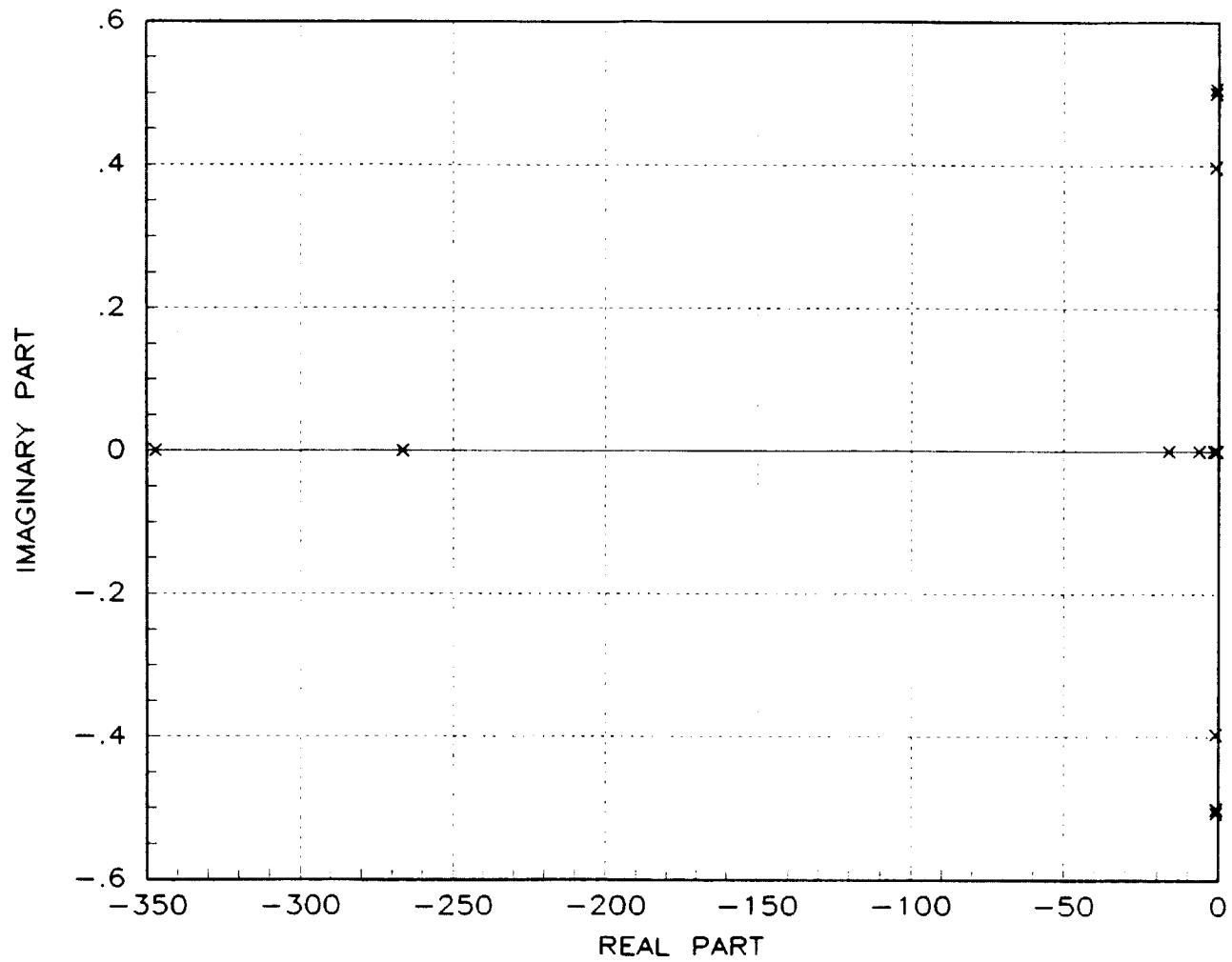


Figure B10.-Closed-loop eigenvalues for the integral feedback system with the model linearized around zero.

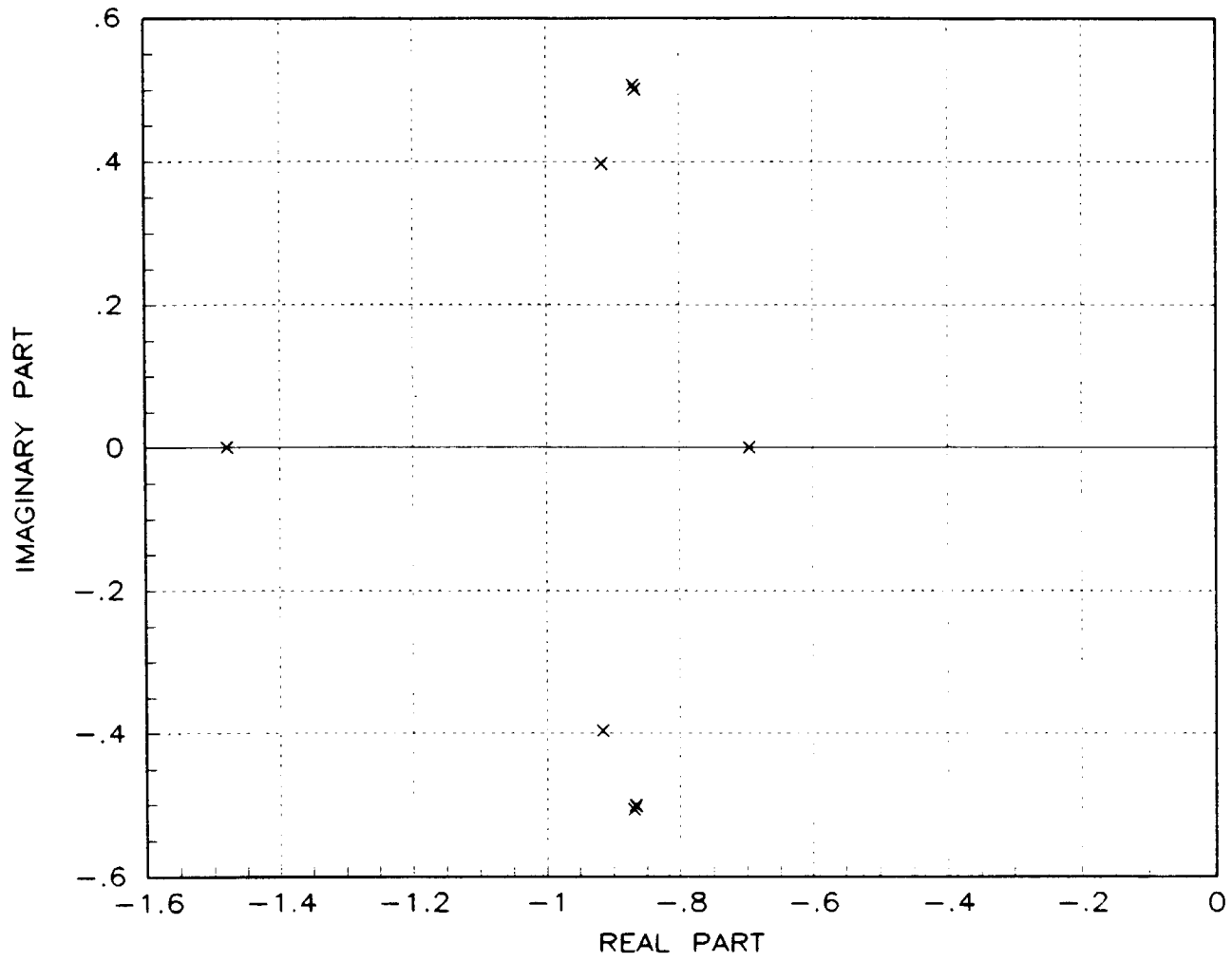


Figure B11.- Low frequency eigenvalues of figure B10.

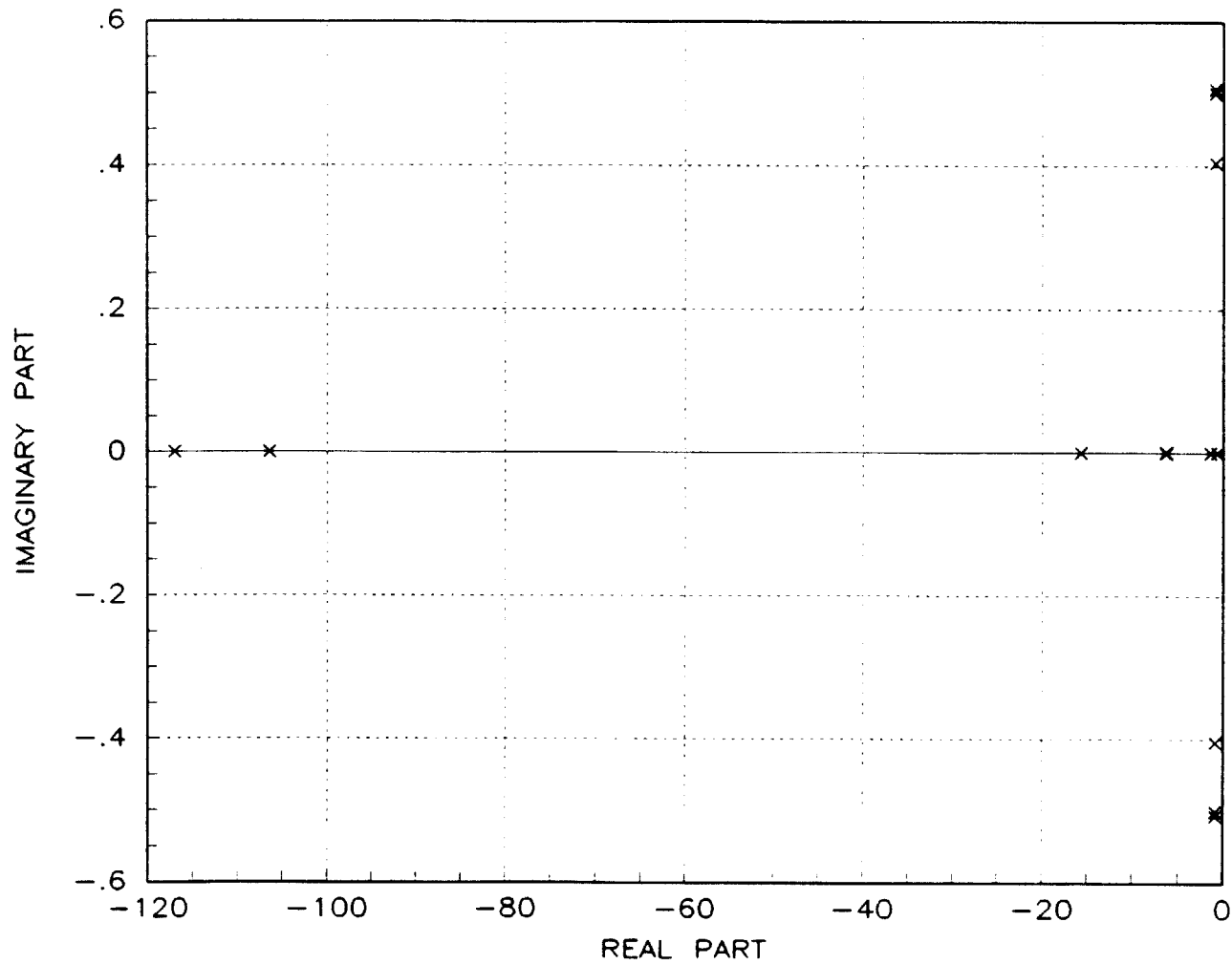


Figure B12.- Closed-loop eigenvalues for the discrete integral feedback system with the model linearized around zero.

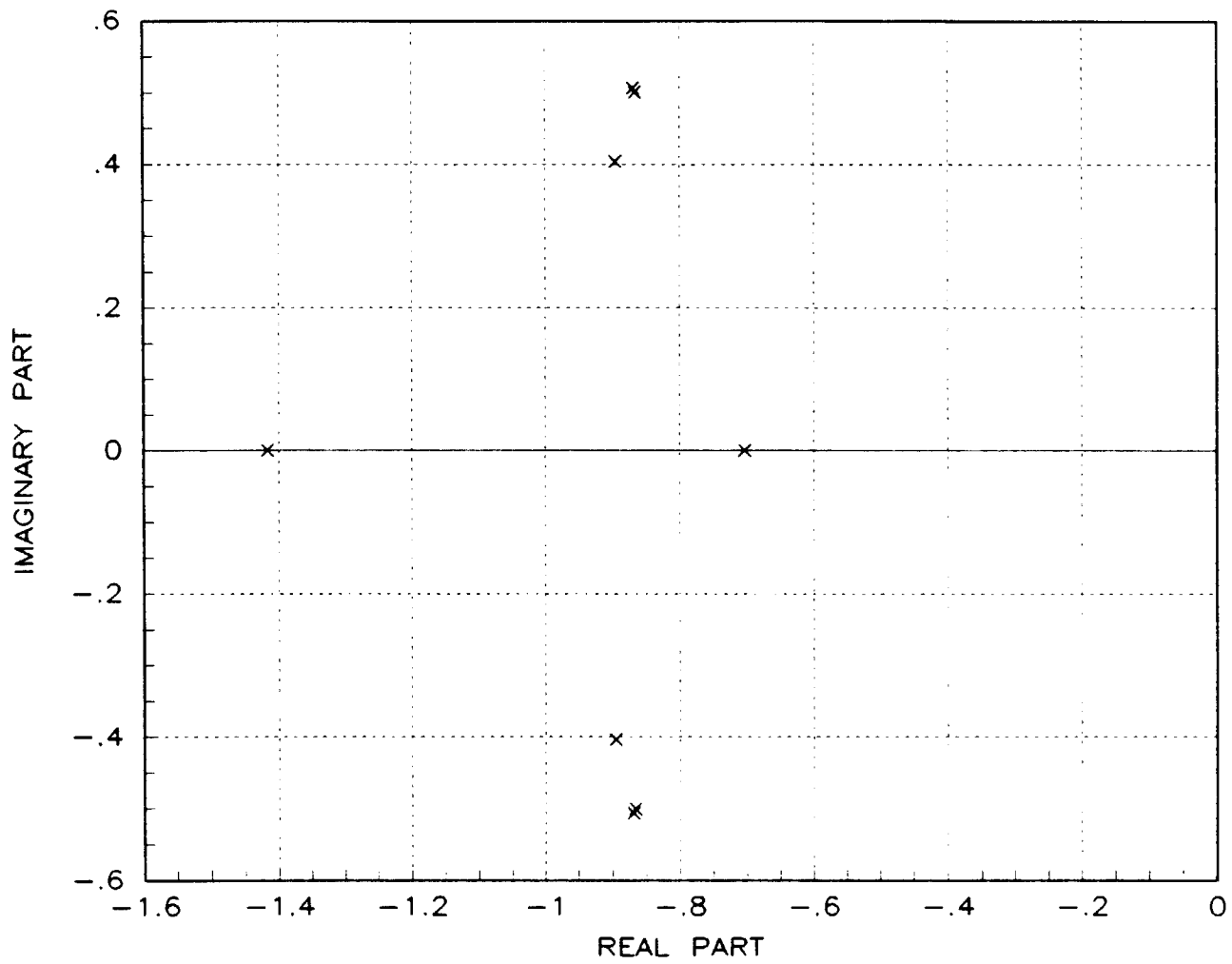


Figure B13.-Low frequency eigenvalues of figure B12.

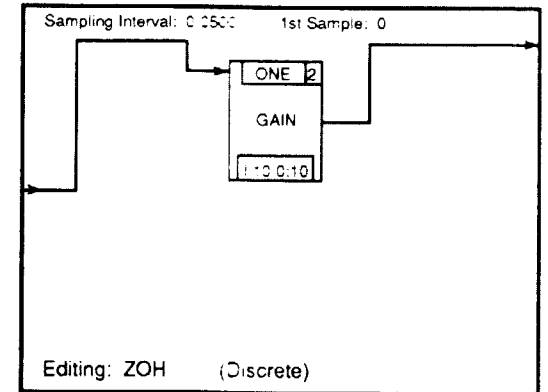
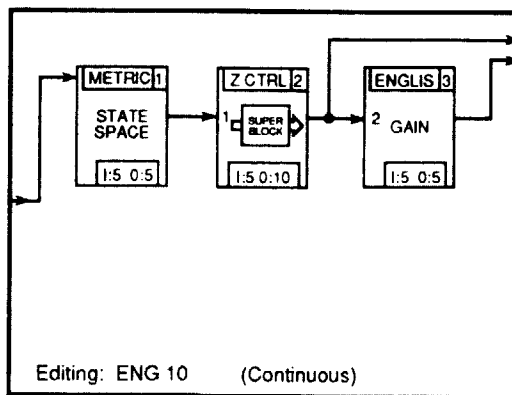
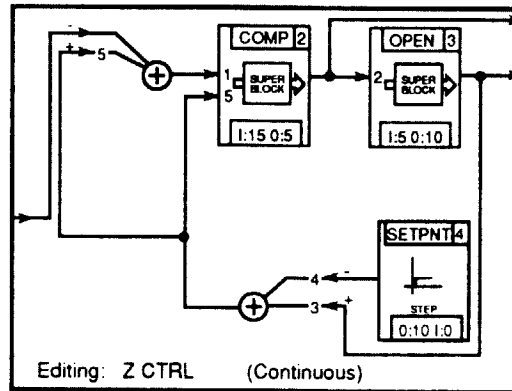
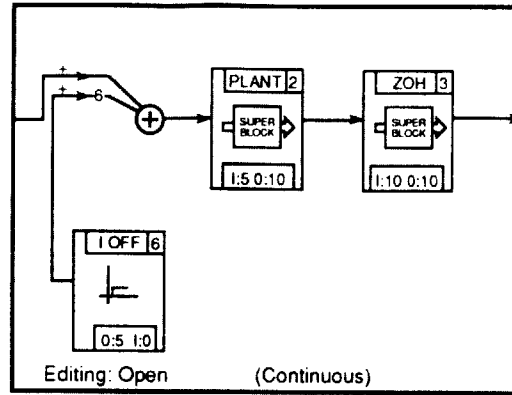
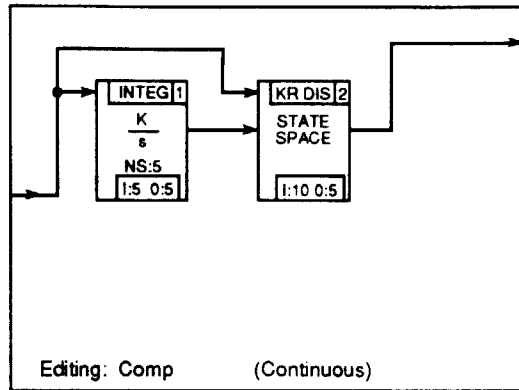


Figure B14.-Super Block implementation of intergral feedback regulator with zero order hold.

REFERENCES

1. Groom, Nelson J.: Analytical Model Of A Five Degree Of Freedom Magnetic Suspension And Positioning System. NASA TM-100671, March 1989.
2. Kwakernaak, Huibert; and Sivan, Raphael: Linear Optimal Control Systems. John Wiley & Sons, Inc., 1972.
3. MATRIX_X User's Guide, Version 6.0. Integrated Systems Inc., 1986.
4. SYSTEM-BUILD User's Guide, Version 6.0. Integrated Systems Inc., 1986.
5. Britcher, Colin P.: Some Aspects Of Wind Tunnel Magnetic Suspension Systems With Special Application At Large Scales. NASA CR-172154, September 1983.
6. Boom, R. W.; Abdelsalam, M. K.; Eyssa, Y. M.; and McIntosh, G. E.: Repulsive Force Support System Feasibility Study. NASA CR-178400, October 1987.

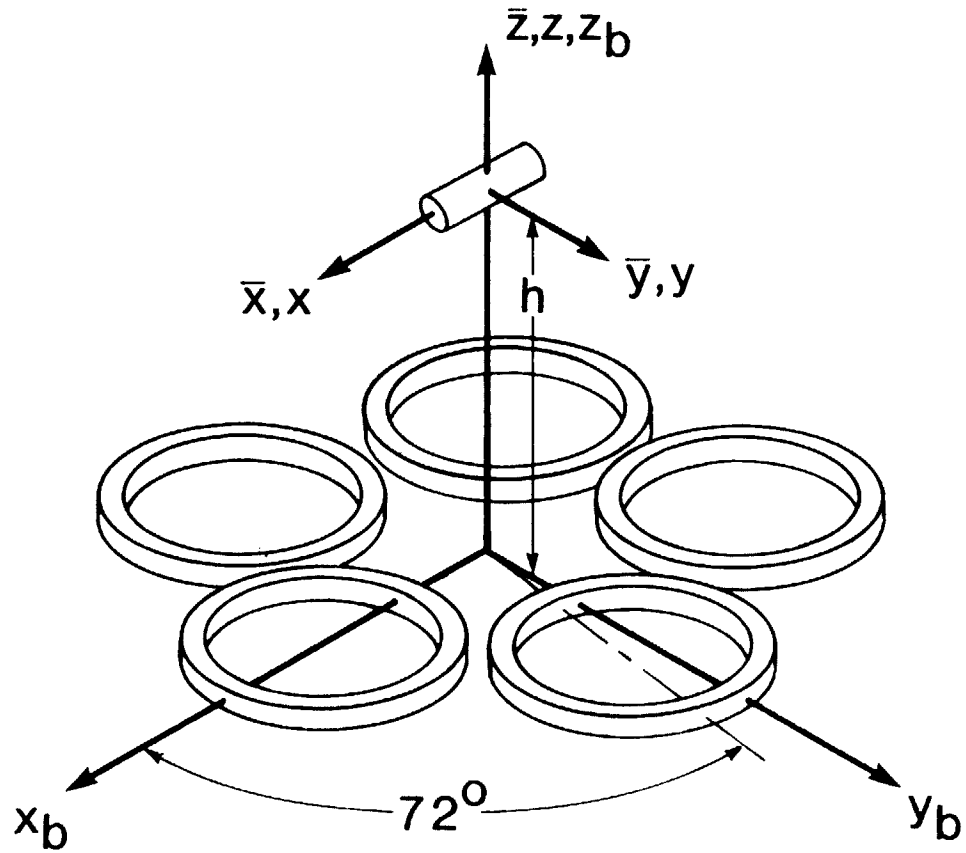


Figure 1.-Initial coordinate system alignment for large gap magnetic suspension system.

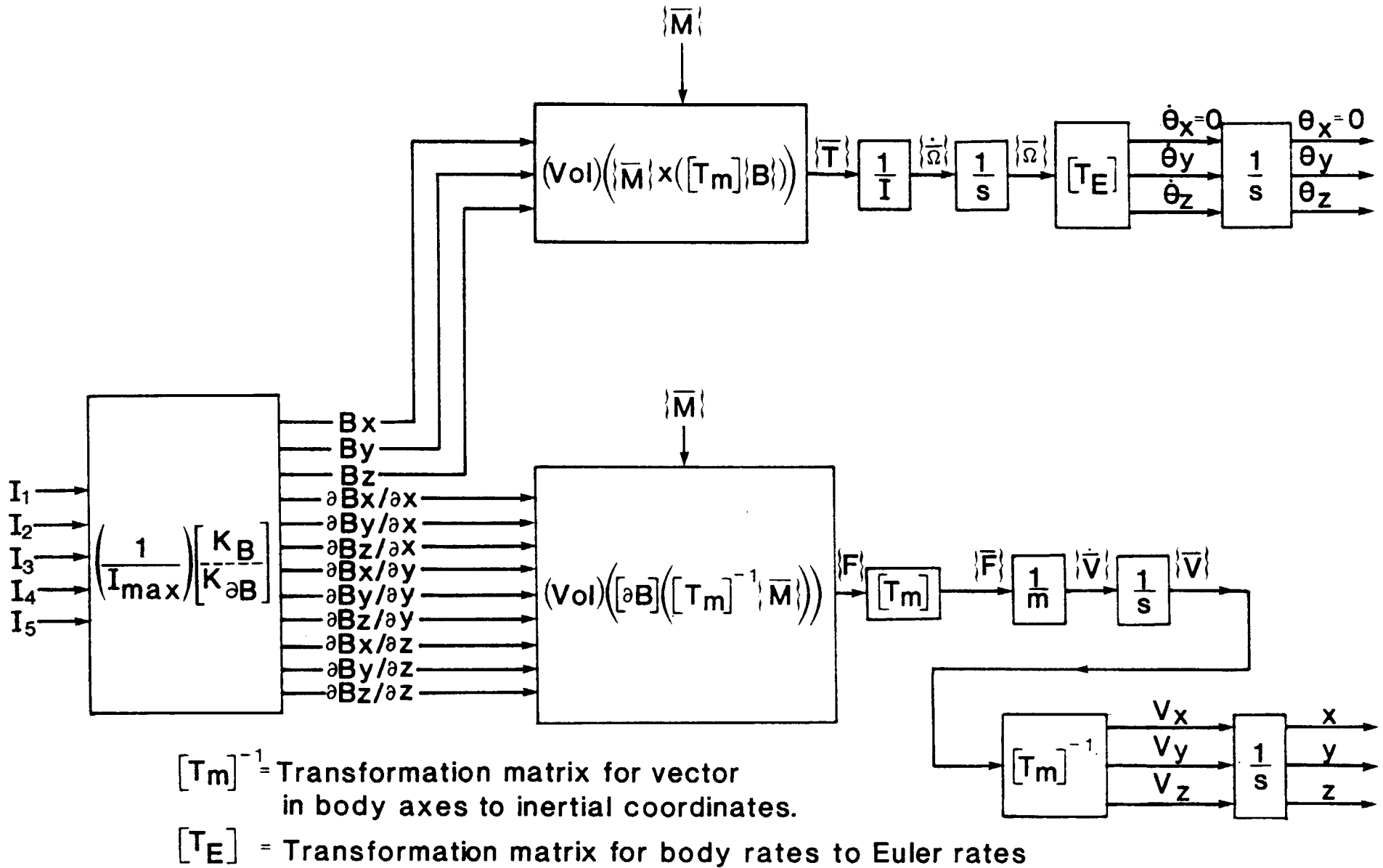


Figure 2.-Block diagram of analytical model of large gap magnetic suspension system.

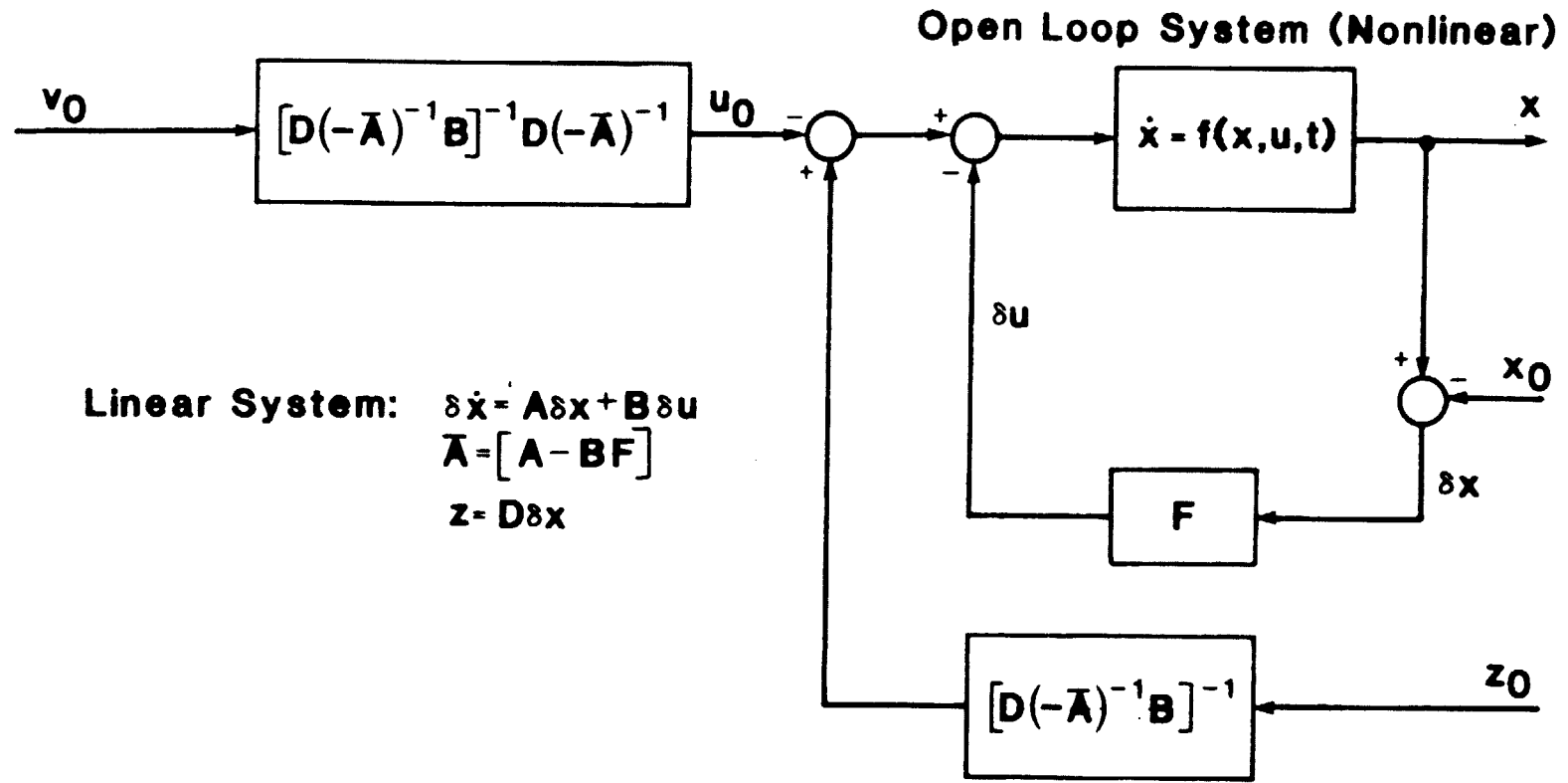


Figure 3.-Nonzero set point regulator.

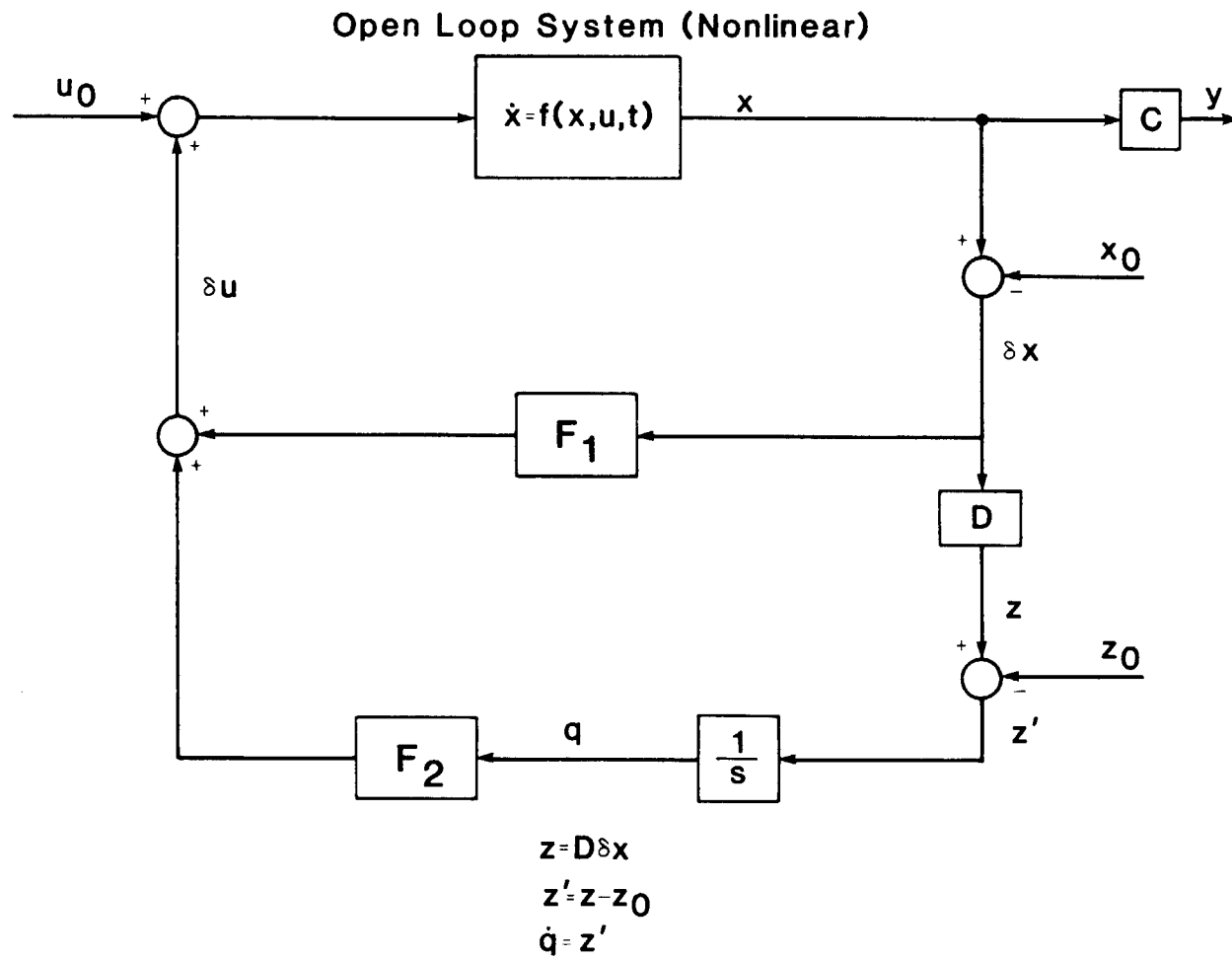


Figure 4.-Integral feedback regulator.

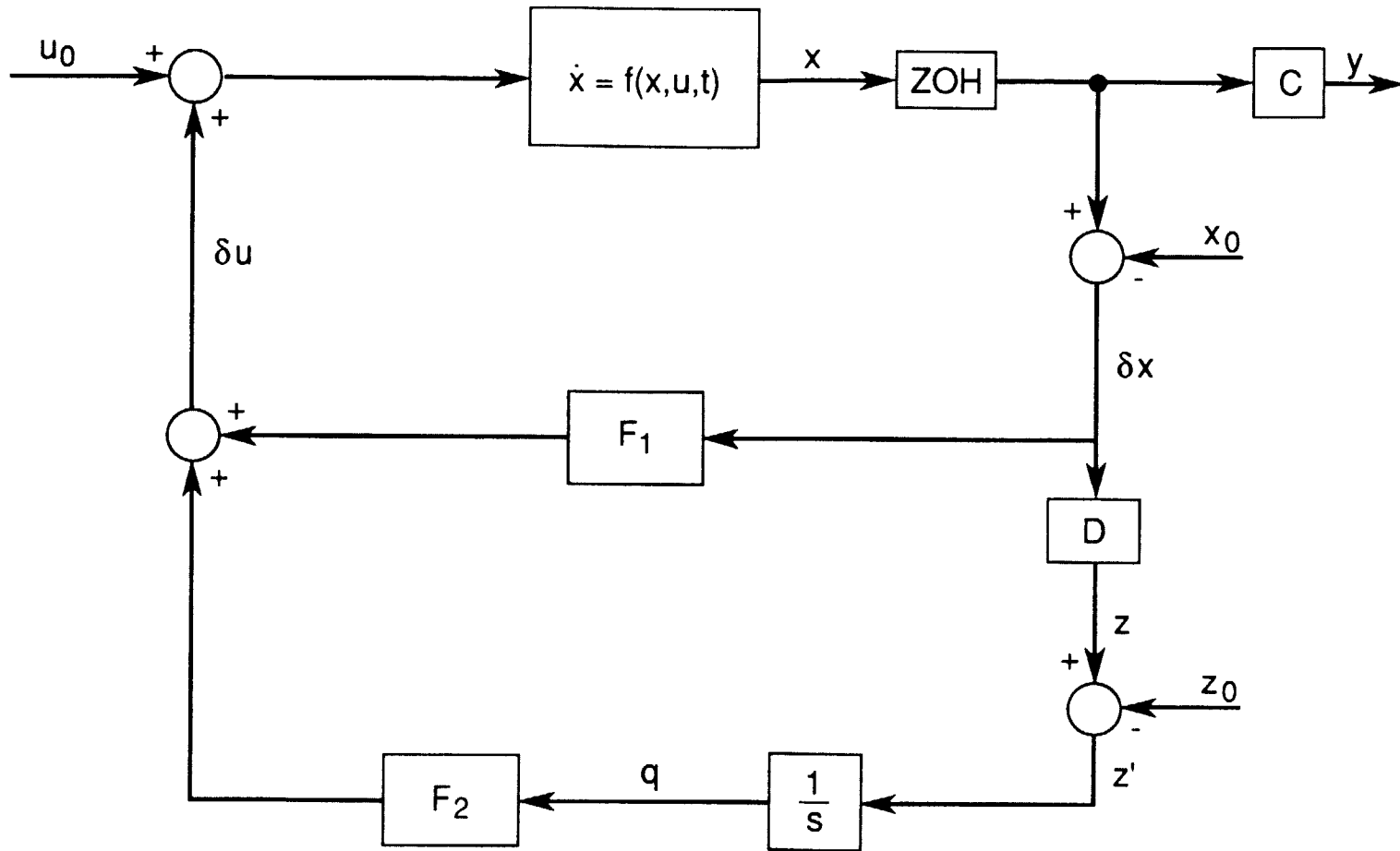


Figure 5.-Integral feedback regulator with zero order hold (ZOH).

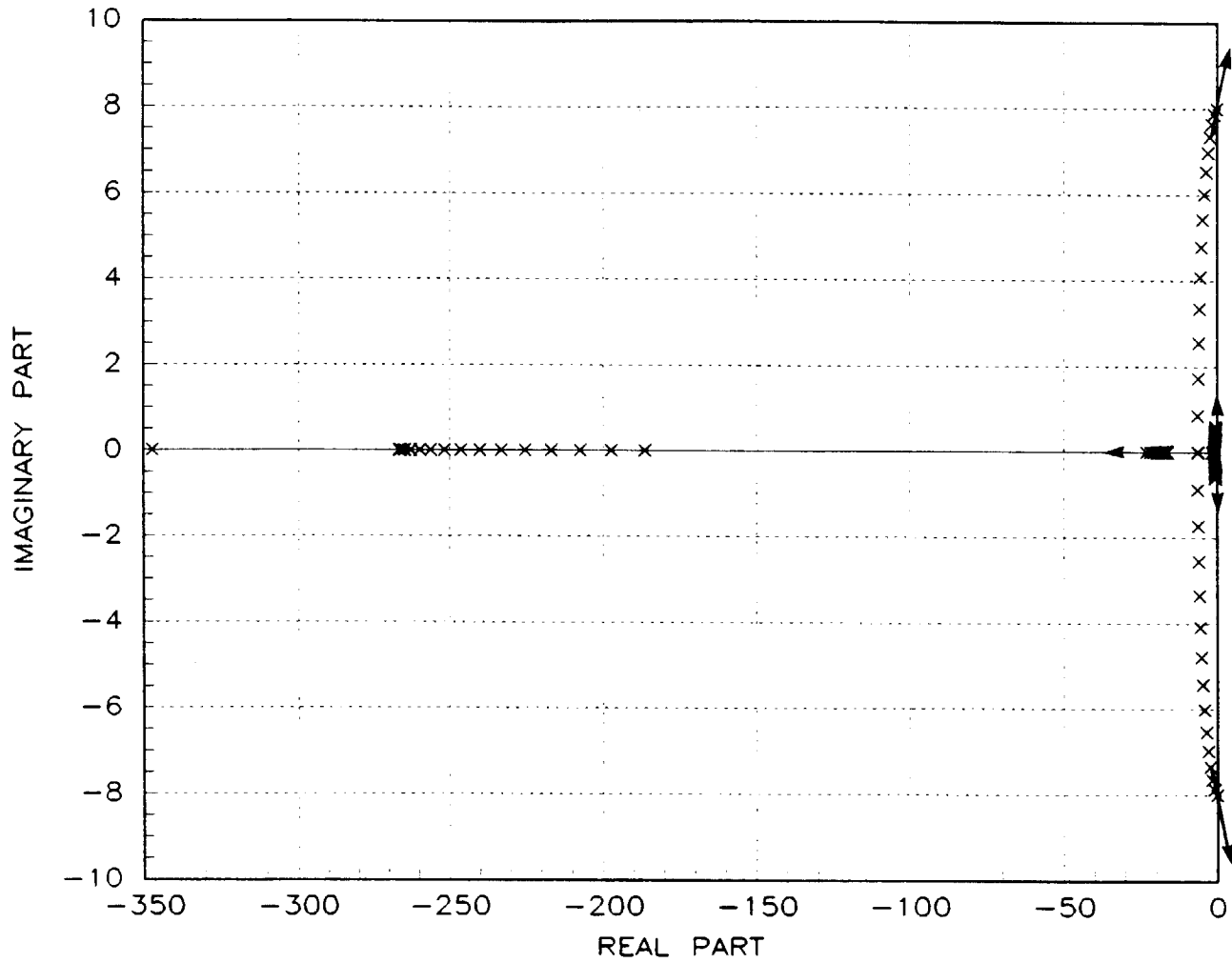


Figure 6.- Eigenvalues of nonzero setpoint regulator with feedback gains calculated at zero yaw angle as core is rotated from zero to 42 degrees yaw in increments of two degrees.

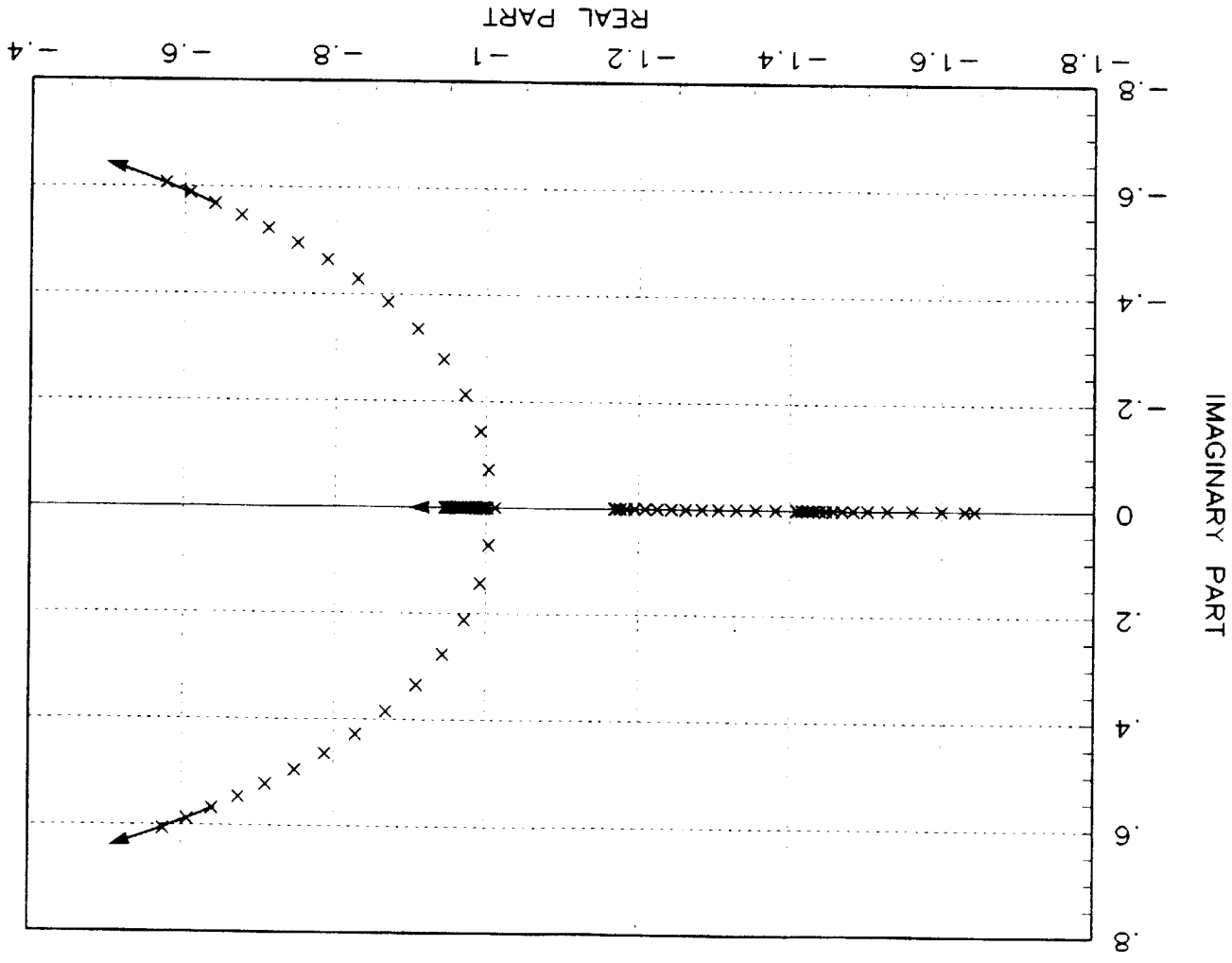


Figure 7.-Low frequency eigenvalues of figure 6.

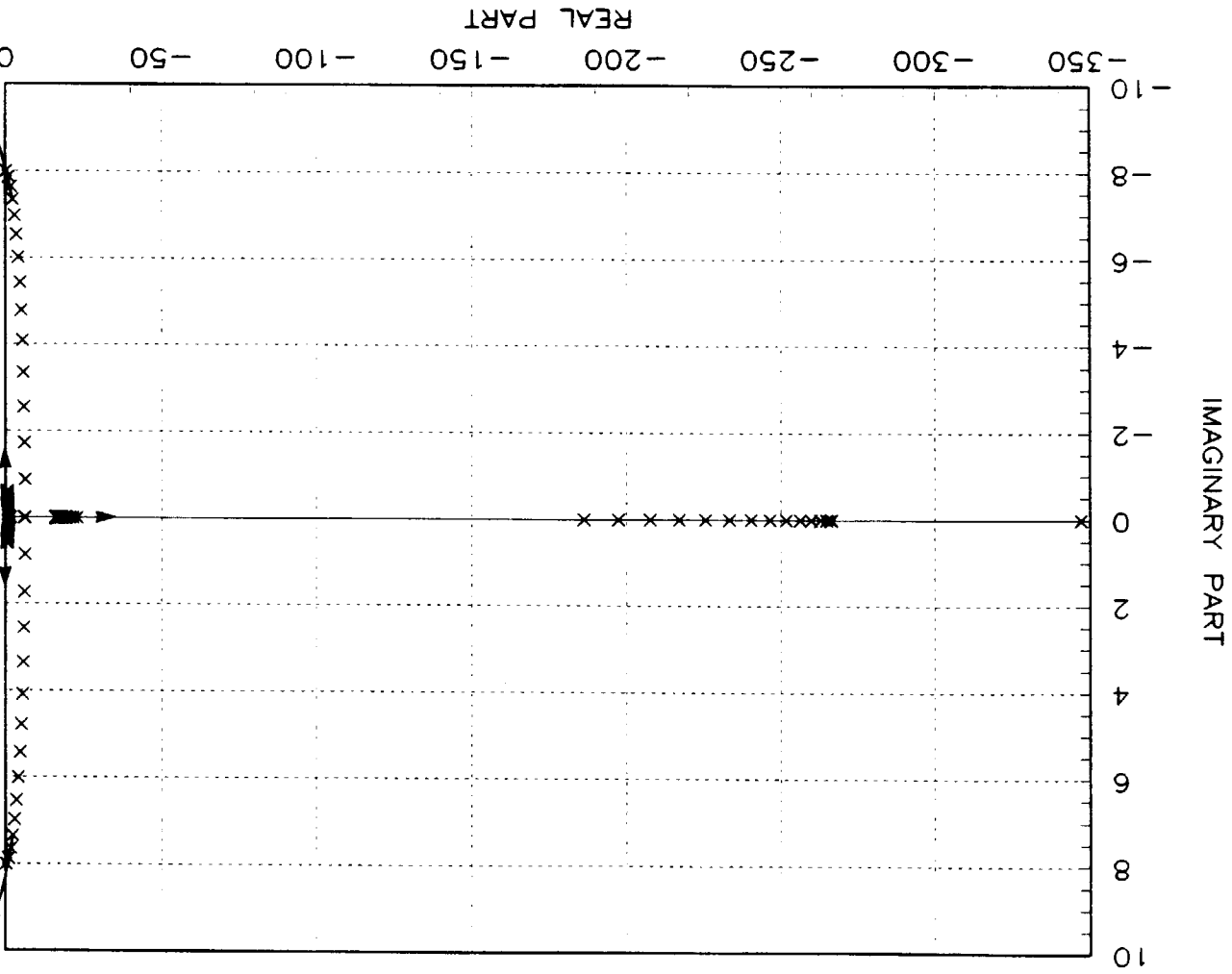


Figure 8 - Eigenvalues of nonzero set point regulator with feedback gains calculated at zero yaw angle as core is rotated from zero to 42 degrees yaw in increments of two degrees.

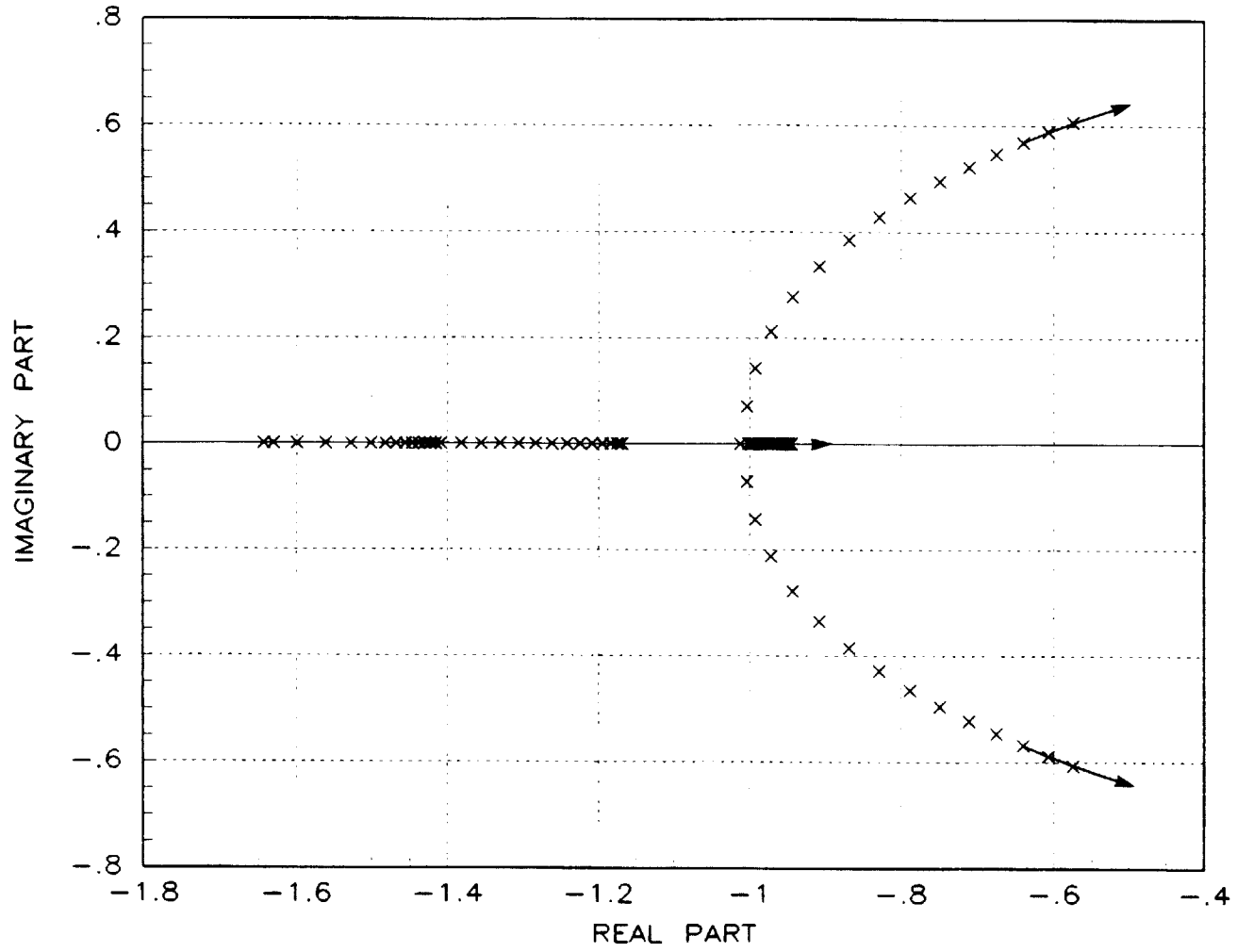


Figure 9.-Low frequency eigenvalues of figure 8.

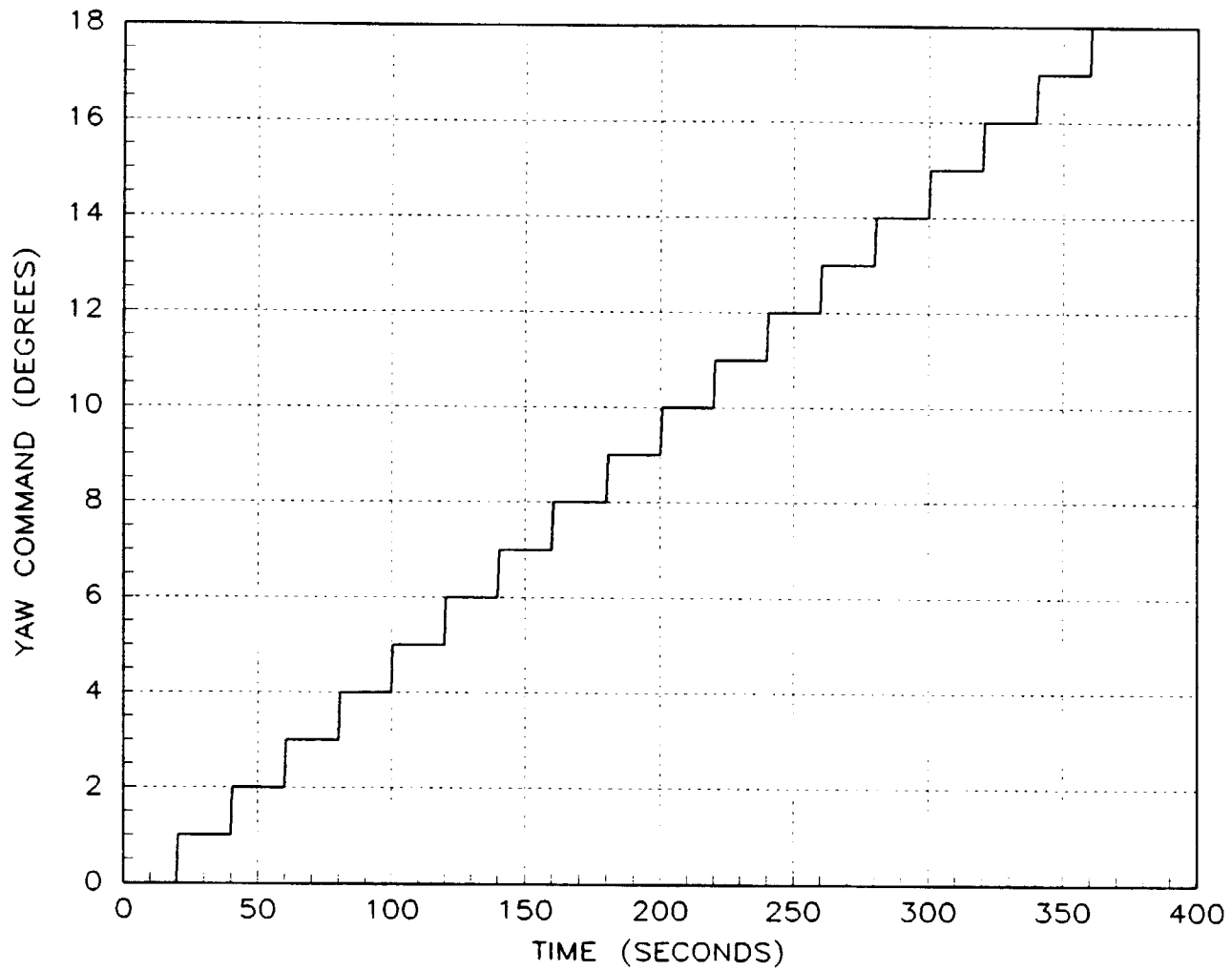


Figure 10.-Input to nonzero set point regulator with feedback gains calculated at zero yaw angle.

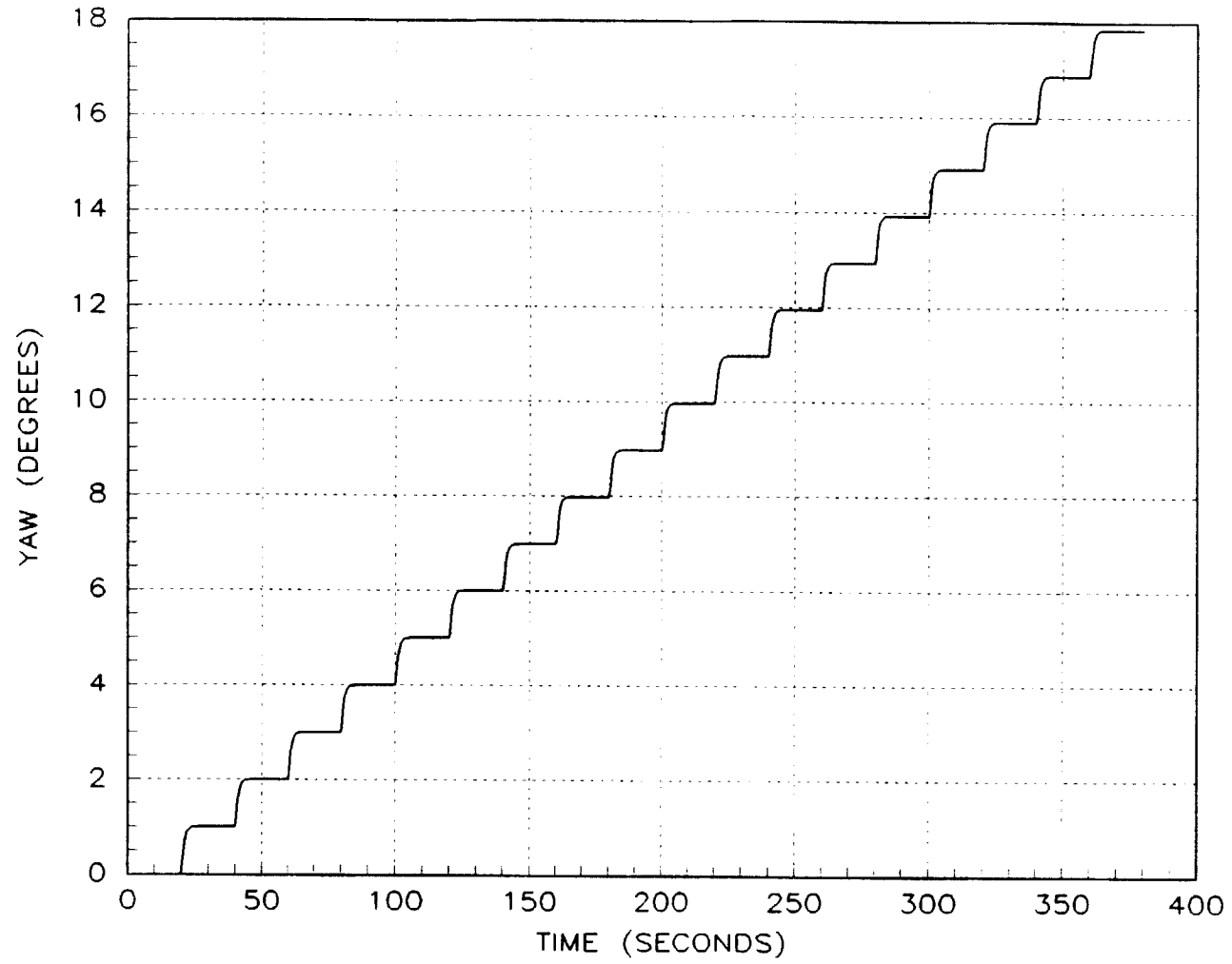


Figure 11.-Yaw angle response to command input of figure 10.

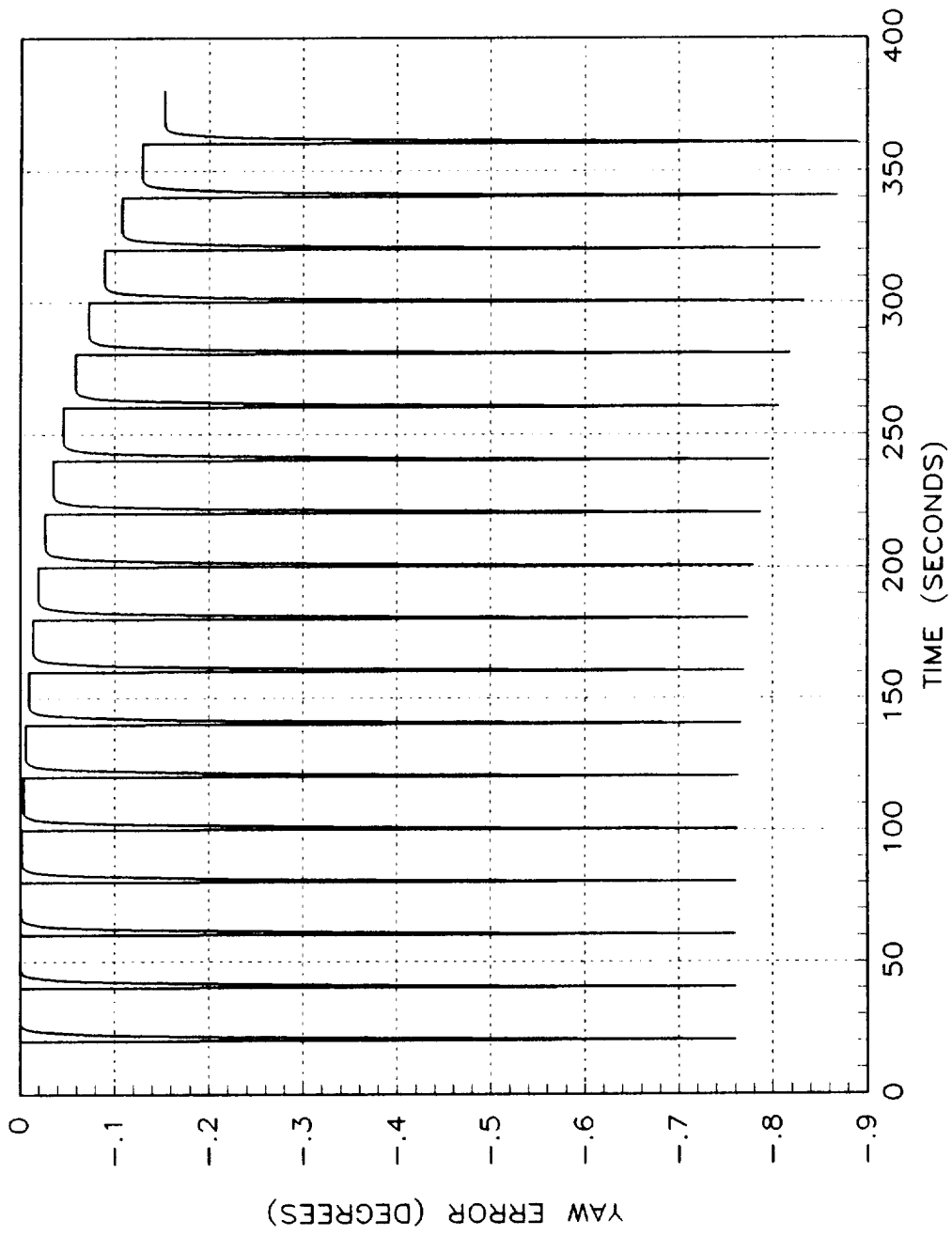


Figure 12.-Difference between command input of figure 10 and response of figure 11.

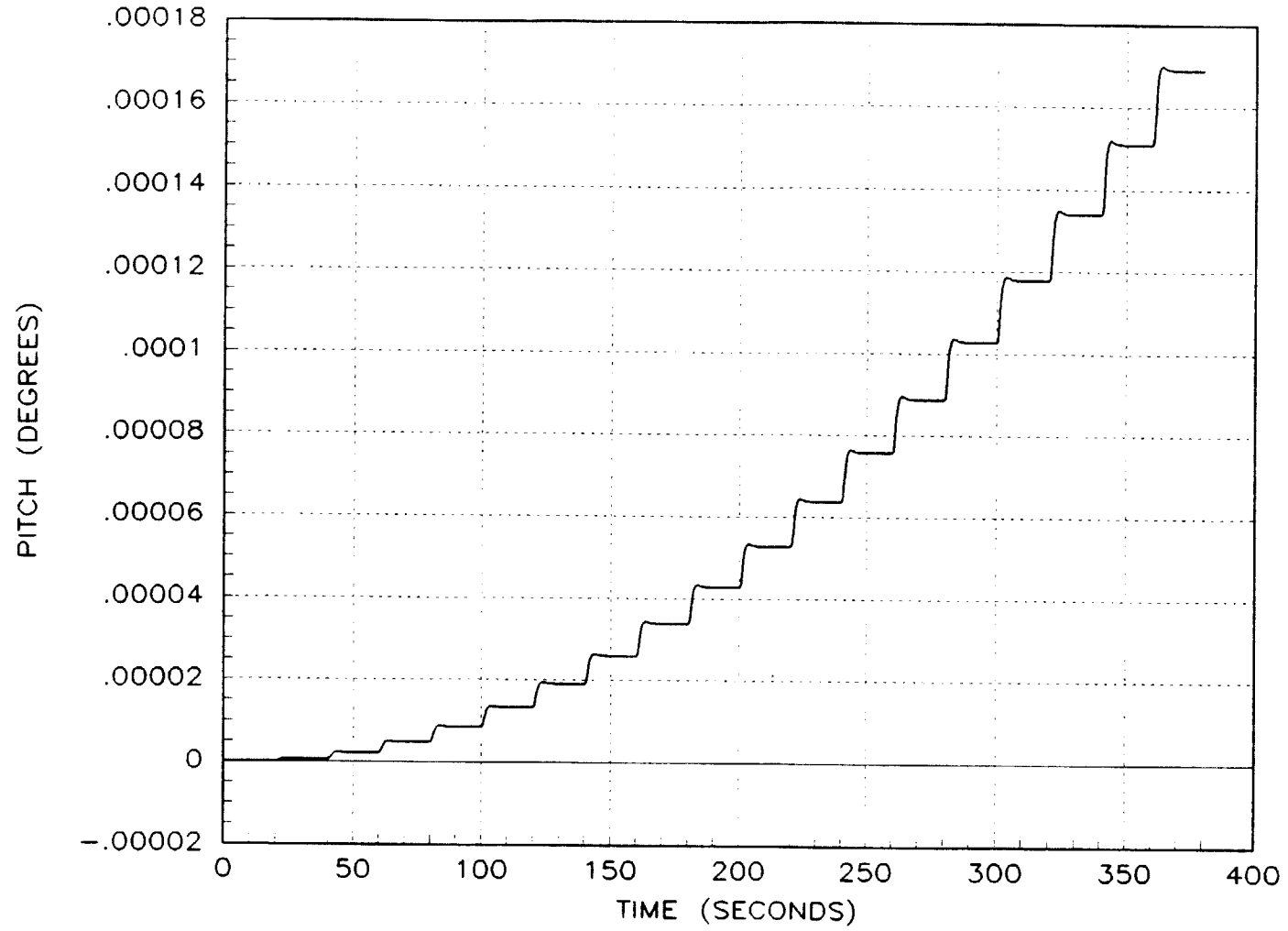


Figure 13.-Pitch angle response to command input of figure 10.

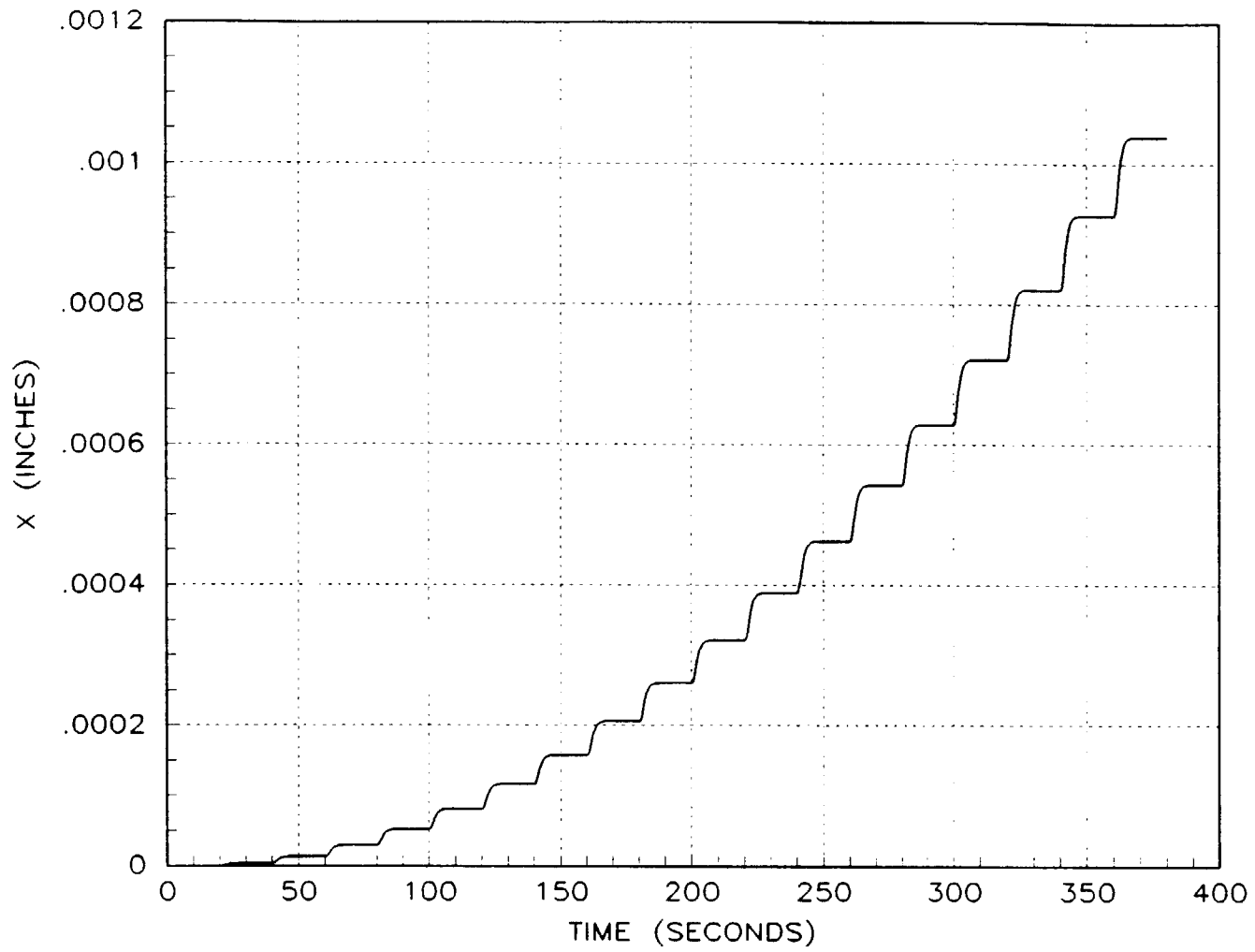


Figure 14.-X axis translational response to command input of figure 10.

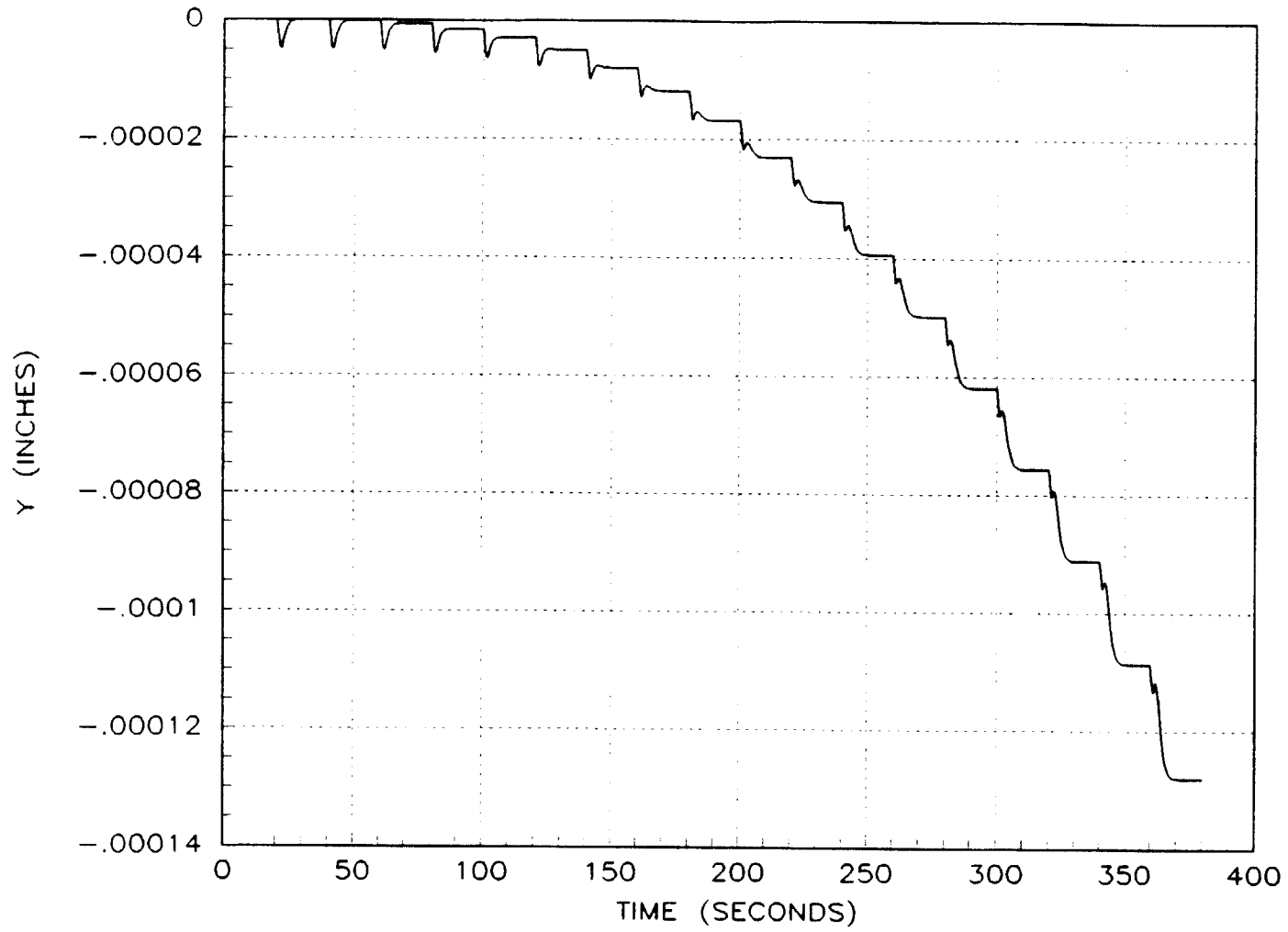


Figure 15.-Y axis translational response to command input of figure 10.

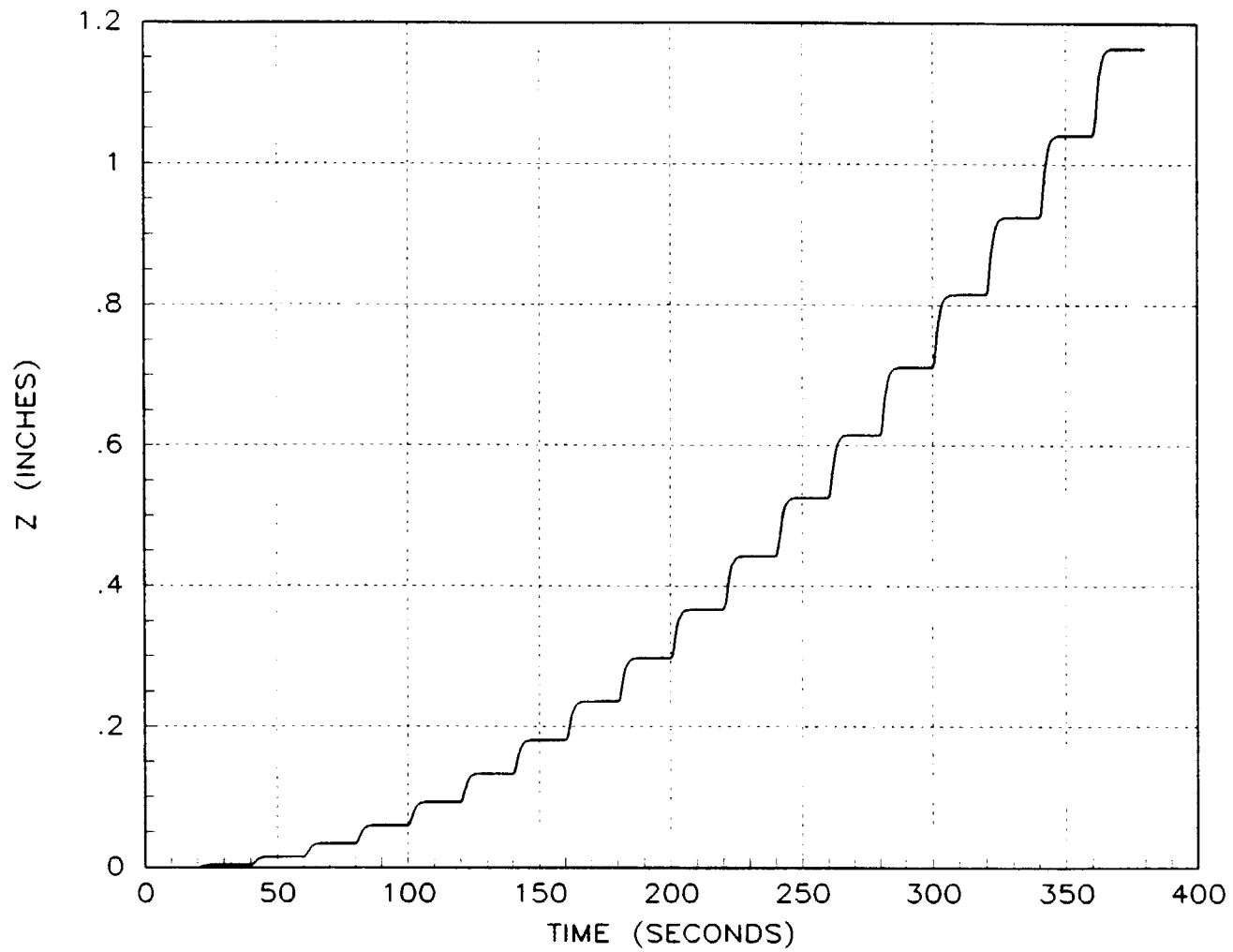


Figure 16.-Z axis translational response to command input of figure 10.

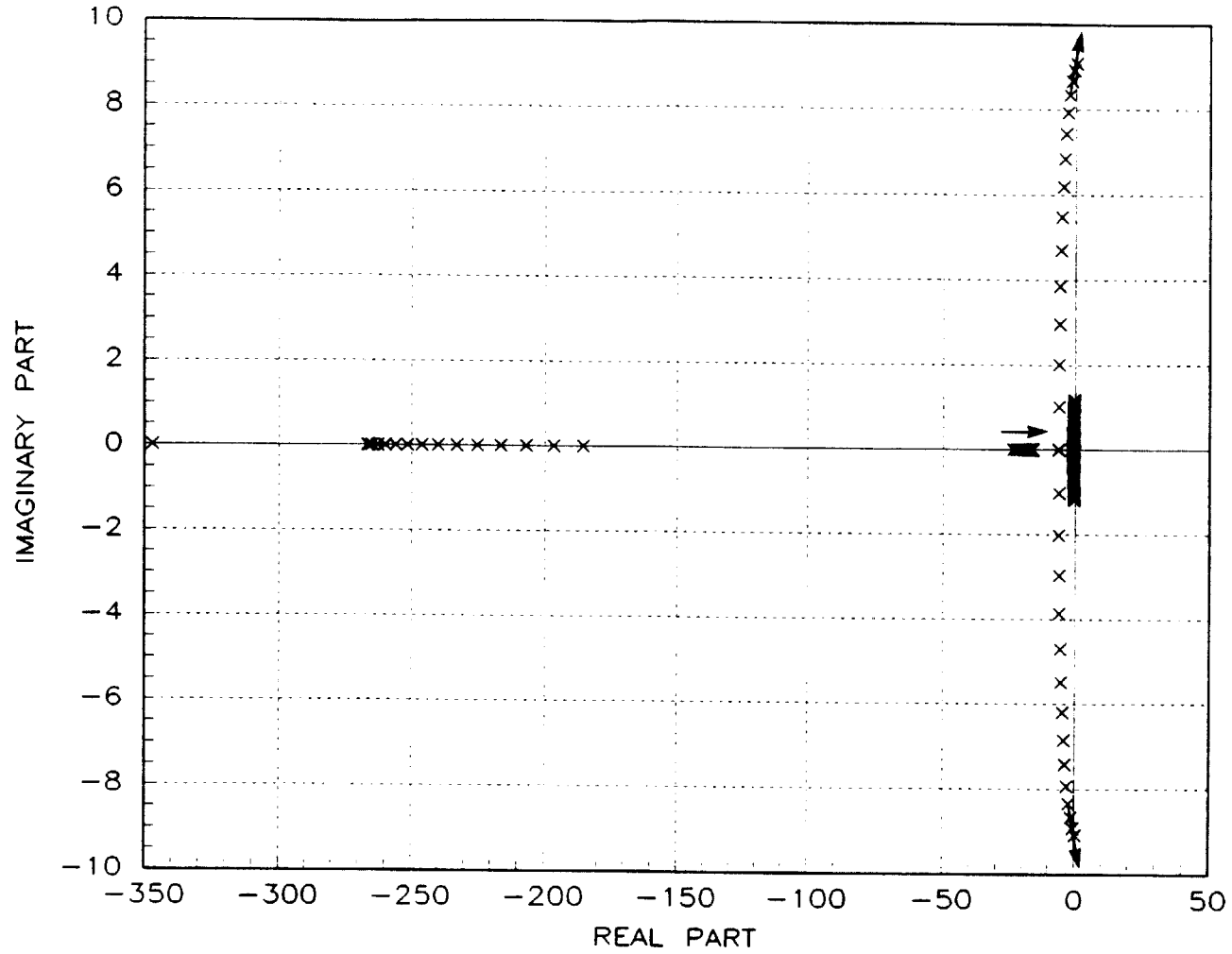


Figure 17.-Eigenvalues of integral feedback regulator with feedback gains calculated at zero yaw angle as core is rotated from zero to 43 degrees in increments of two degrees.

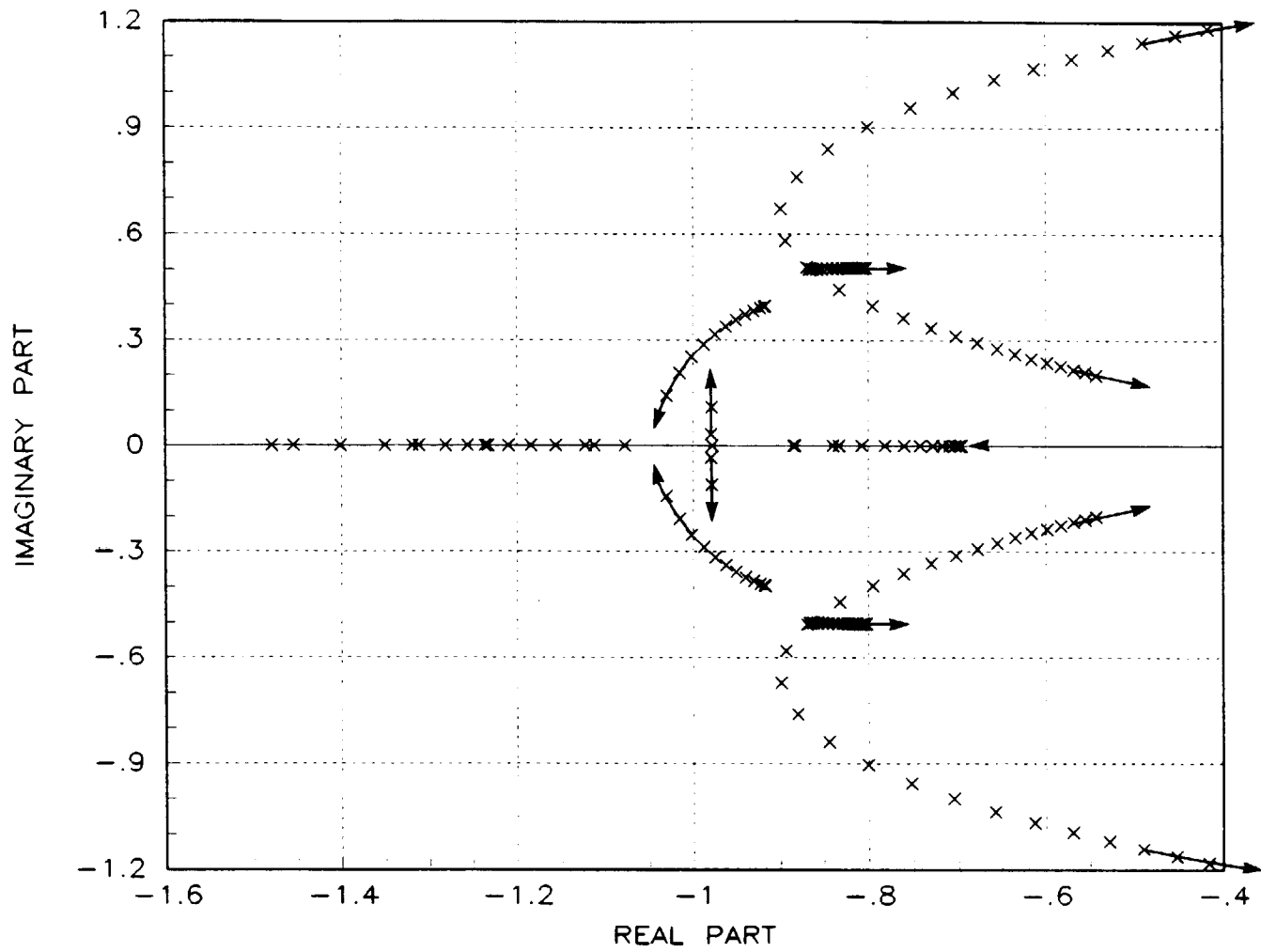


Figure 18.-Low frequency eigenvalues of figure 17.

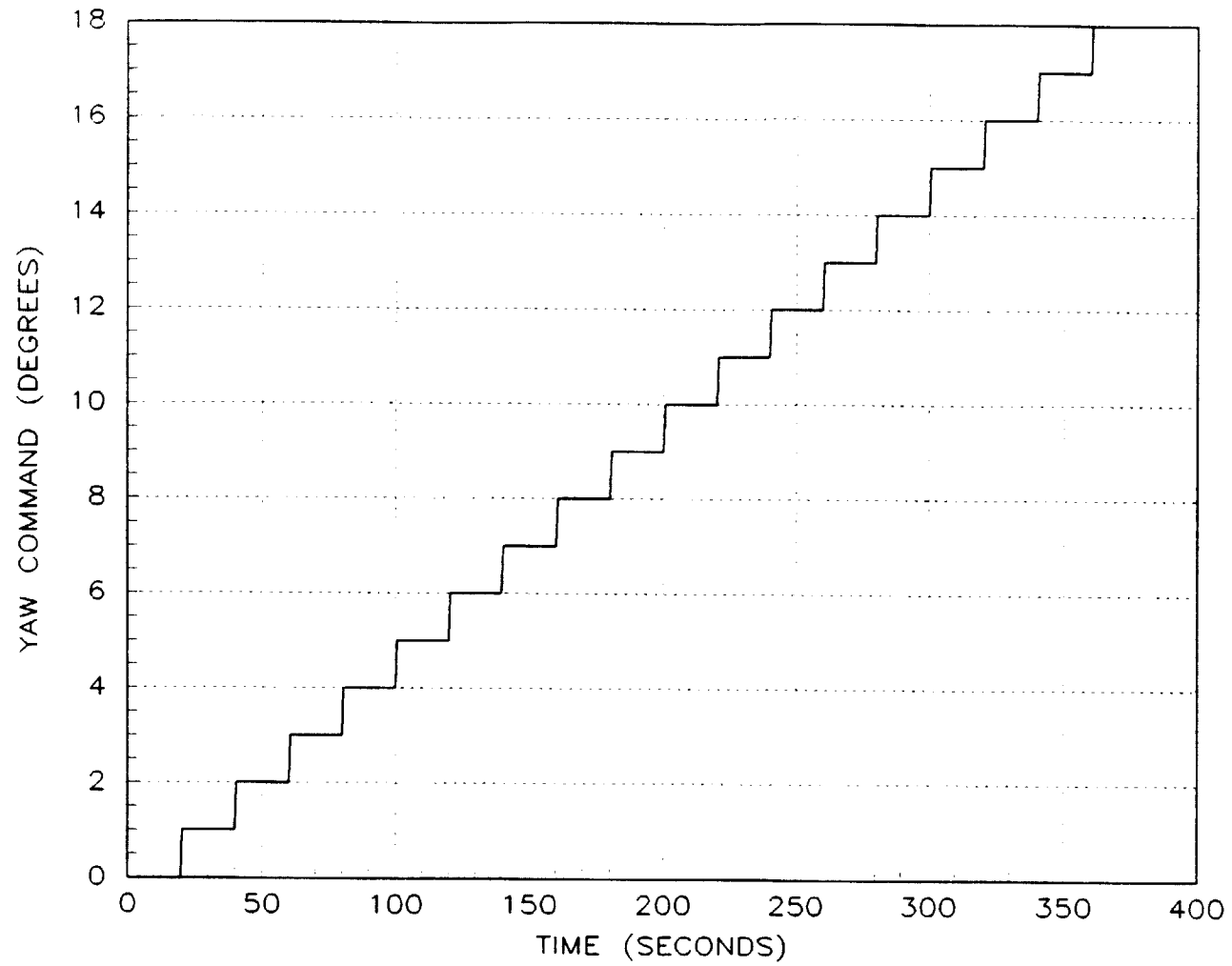


Figure 19.-Input to integral feedback regulator with feedback gains calculated at zero yaw angle.

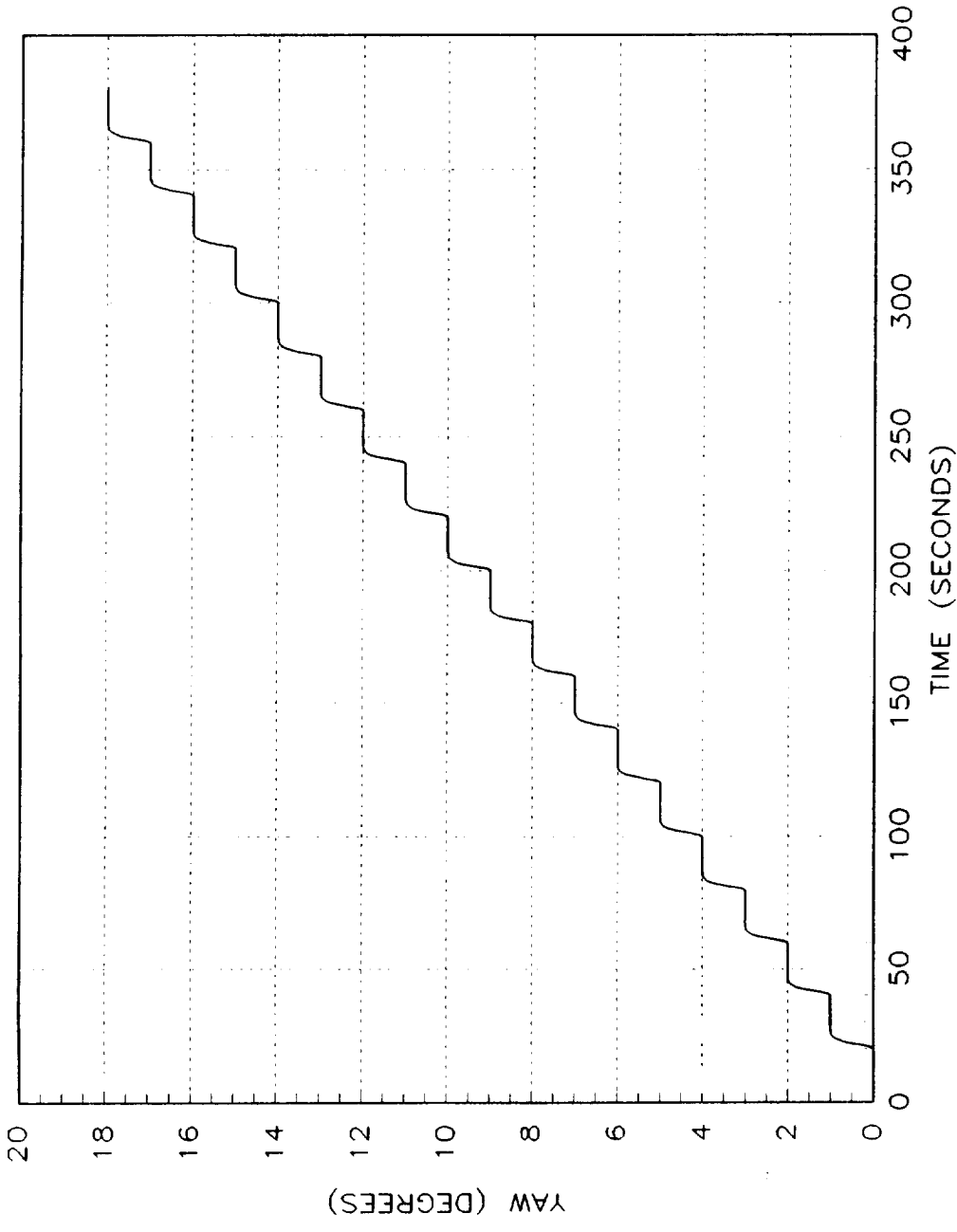


Figure 20.-Yaw angle response to command input of figure 19.

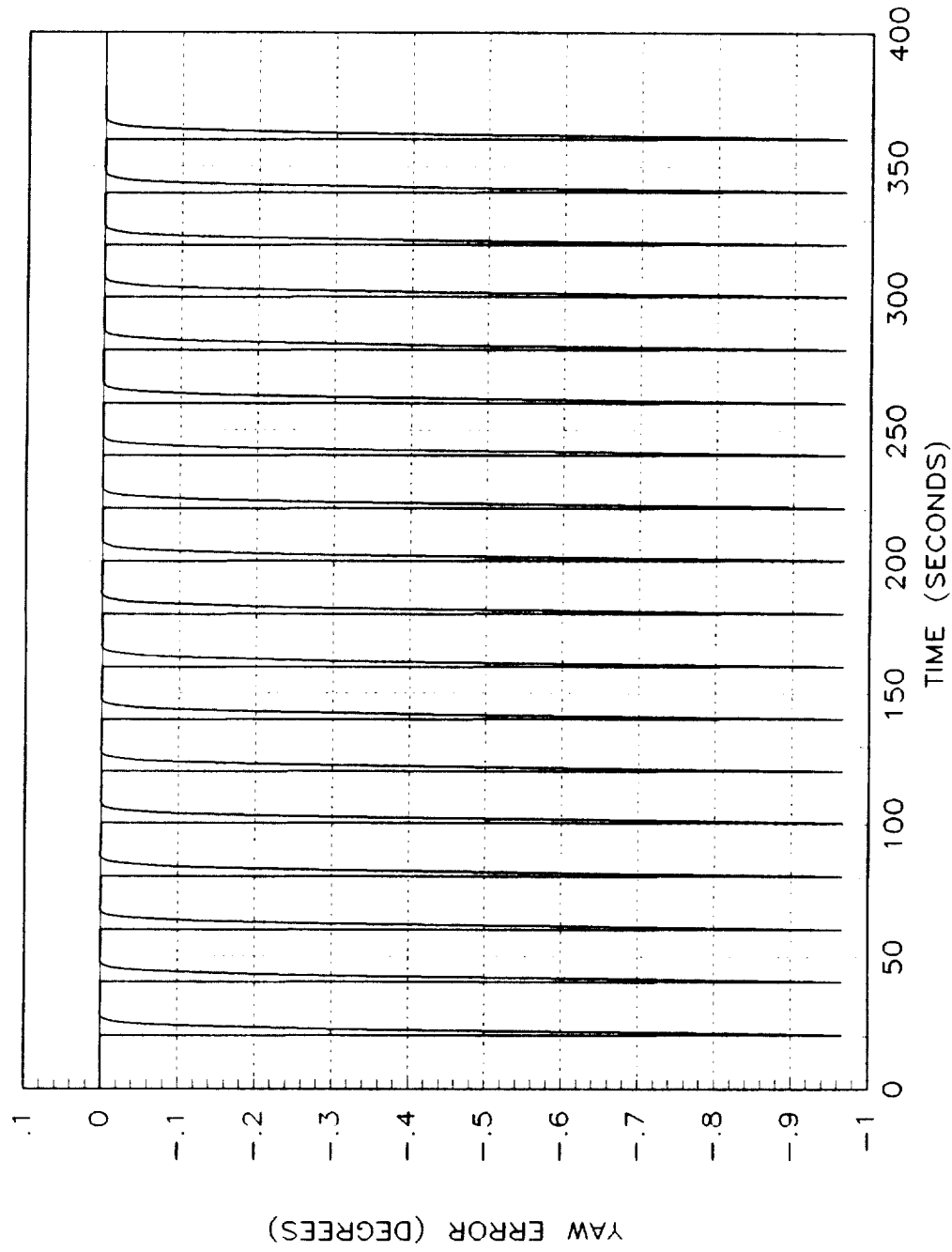


Figure 21.-Difference between command input of figure 19 and response of figure 20.

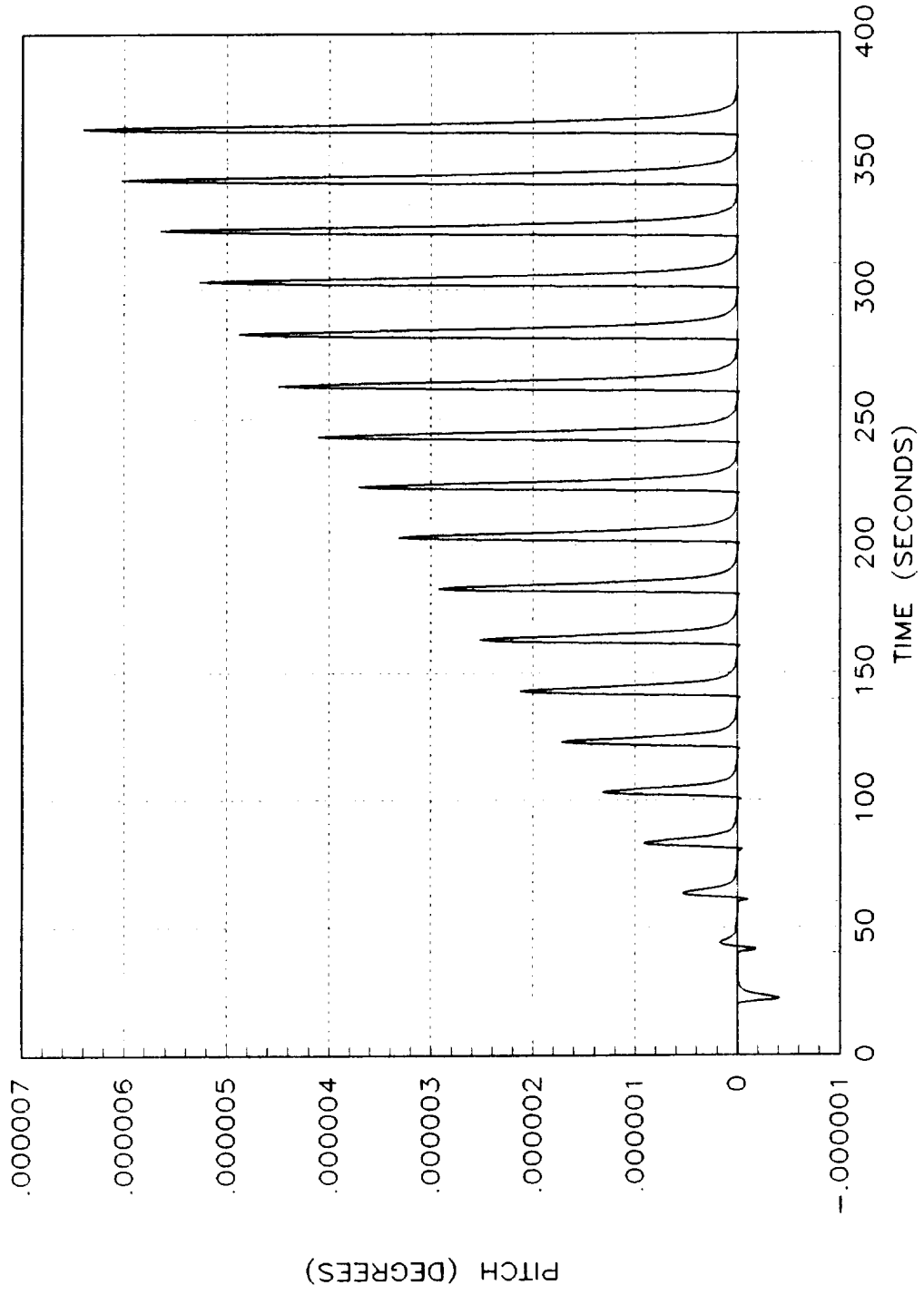


Figure 22.-Pitch angle response to command input of figure 19.

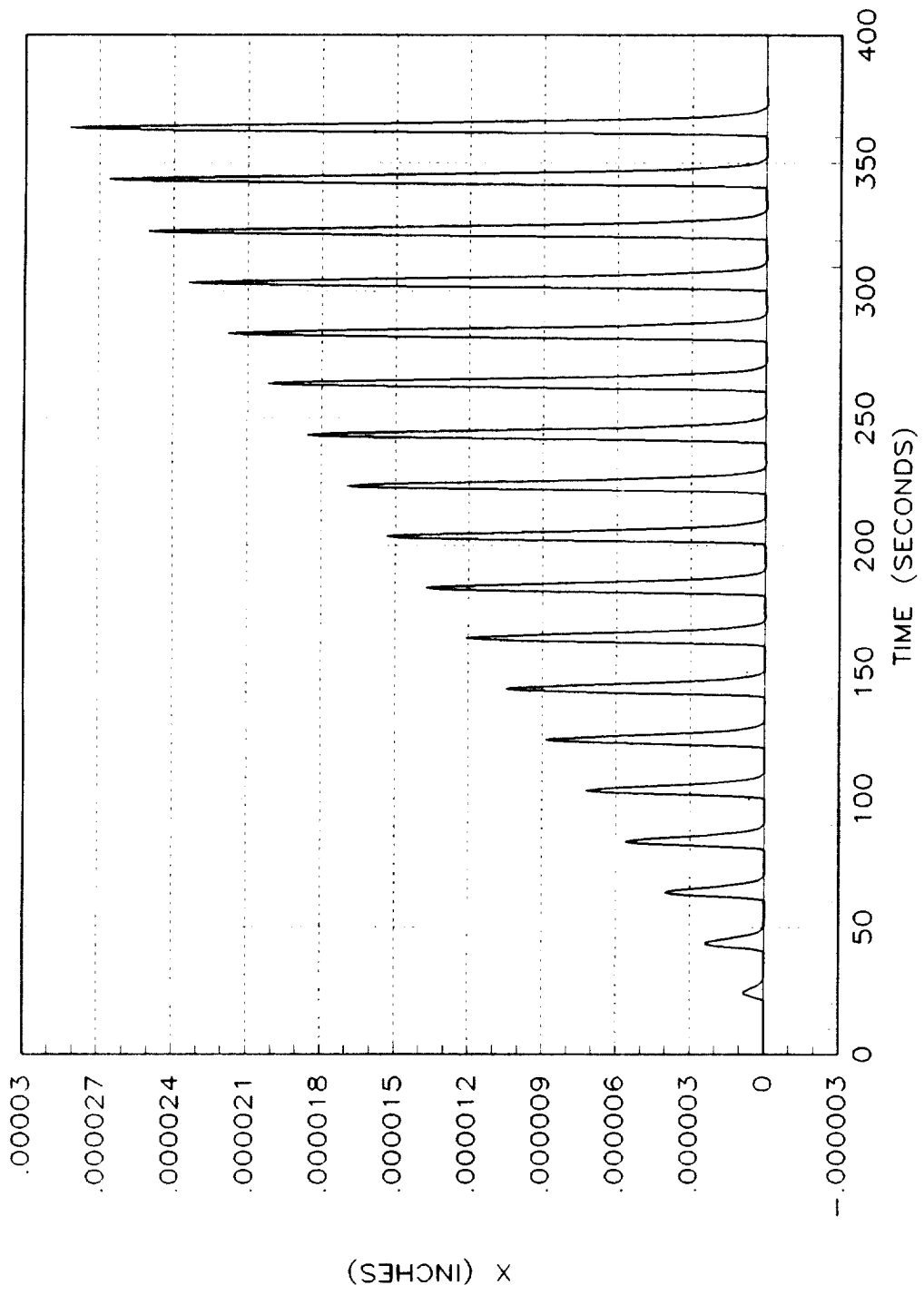


Figure 23.-X axis translational response to command input of figure 19.

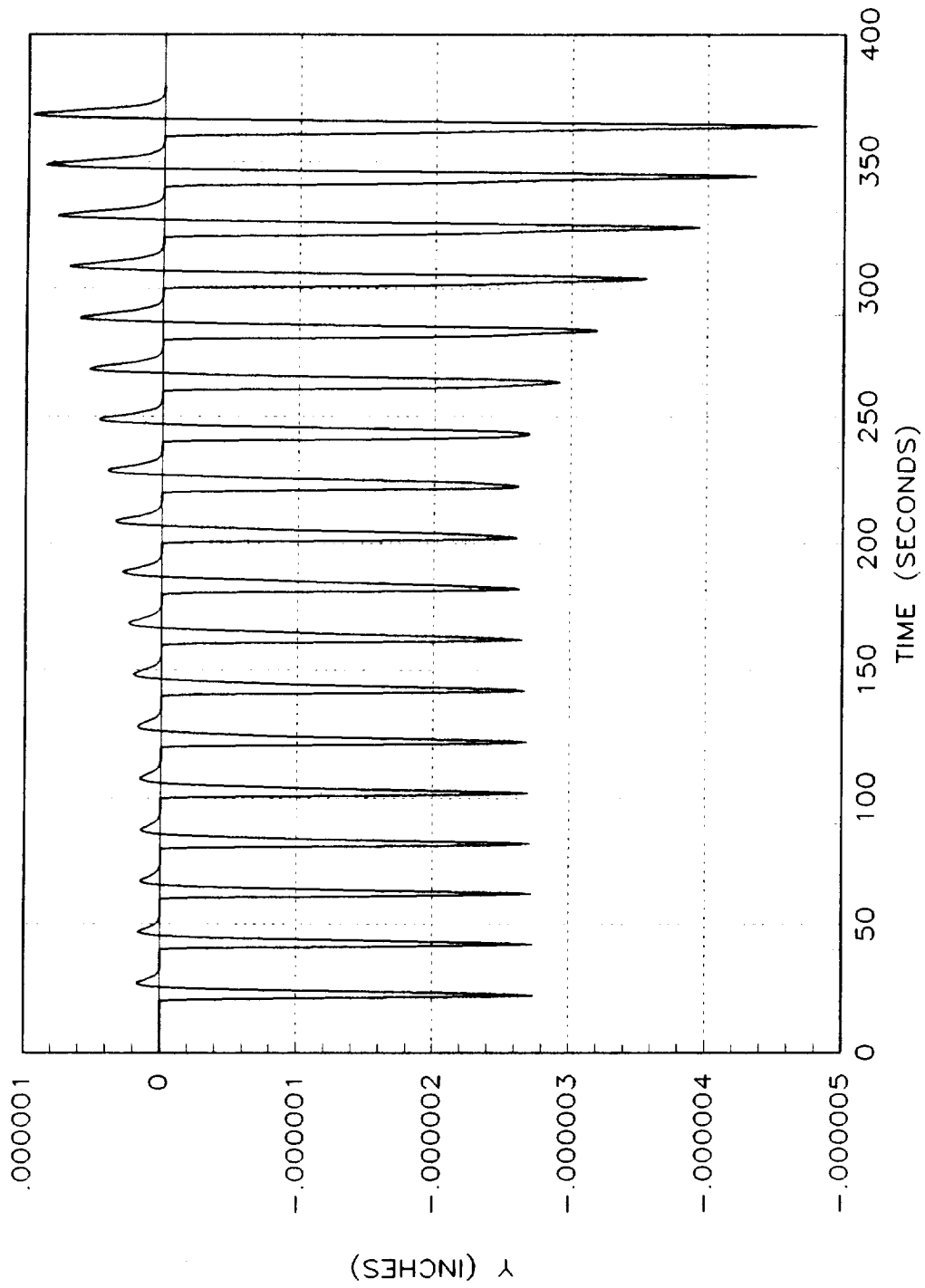


Figure 24.-Y axis translational response to command input of figure 19.

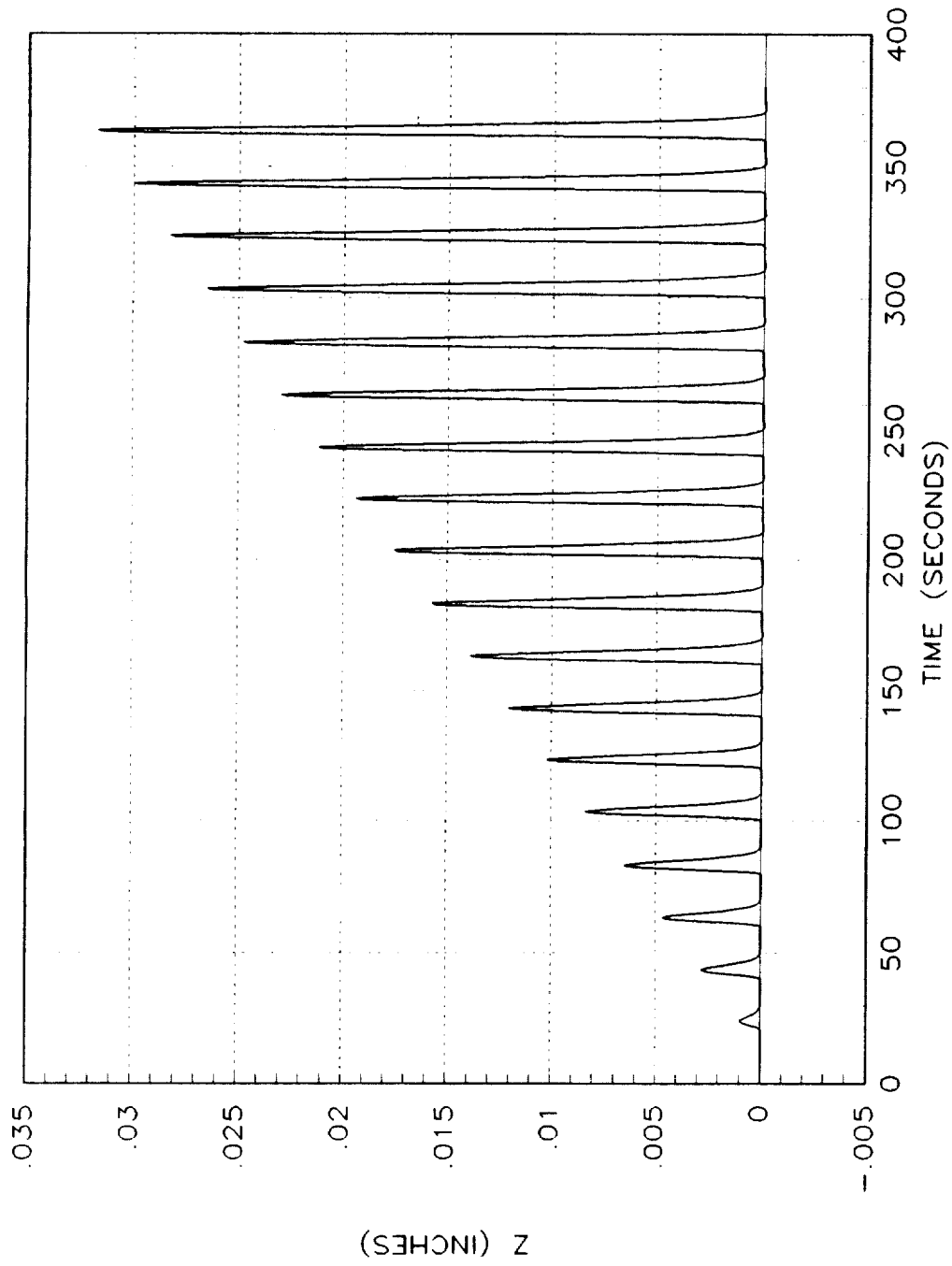


Figure 25.-Z axis translational response to command input of figure 19.

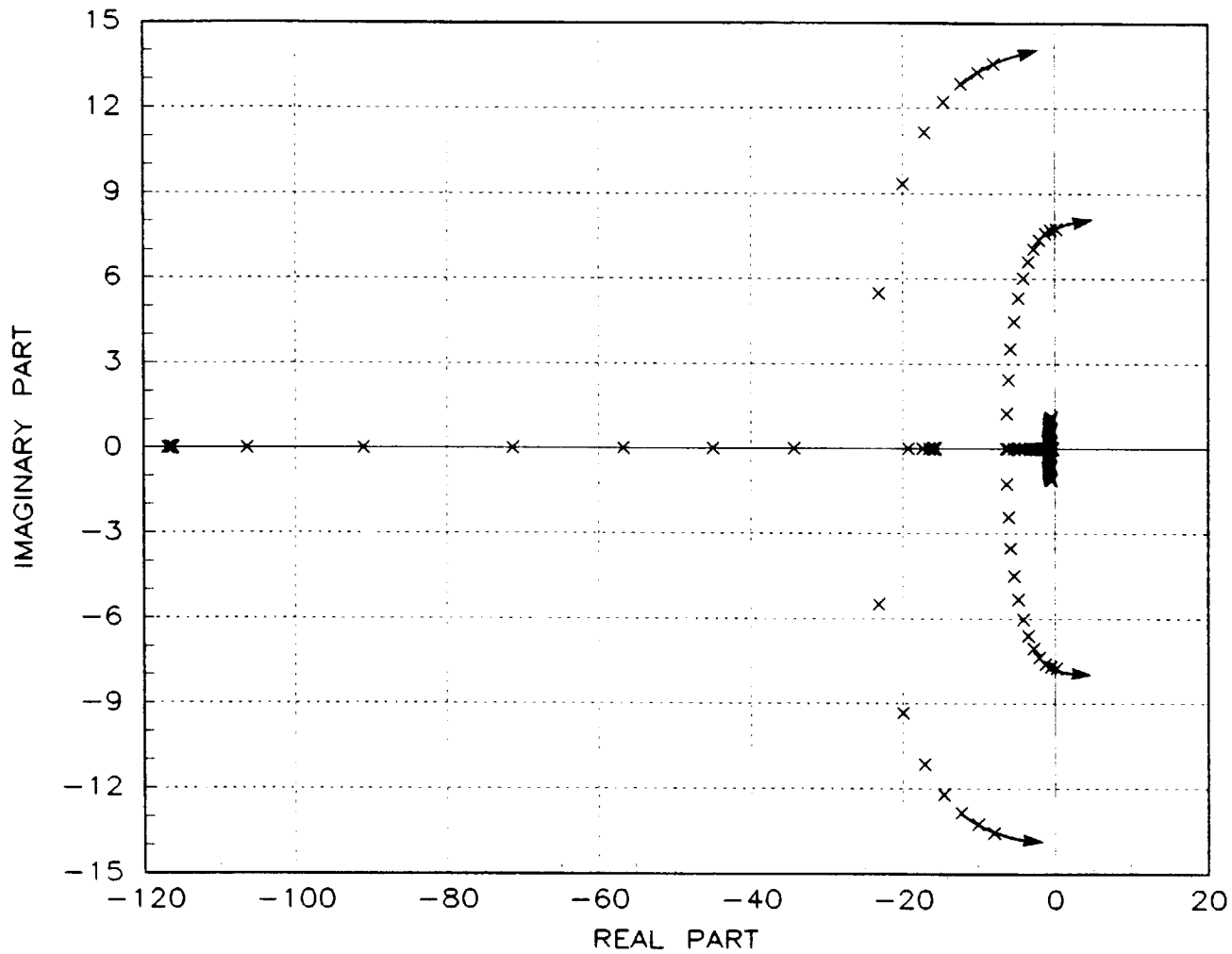


Figure 26.-Eigenvalues of discrete integral feedback regulator with feedback gains calculated at zero yaw angle as core is rotated from zero to 36 degrees yaw in increments of two degrees.

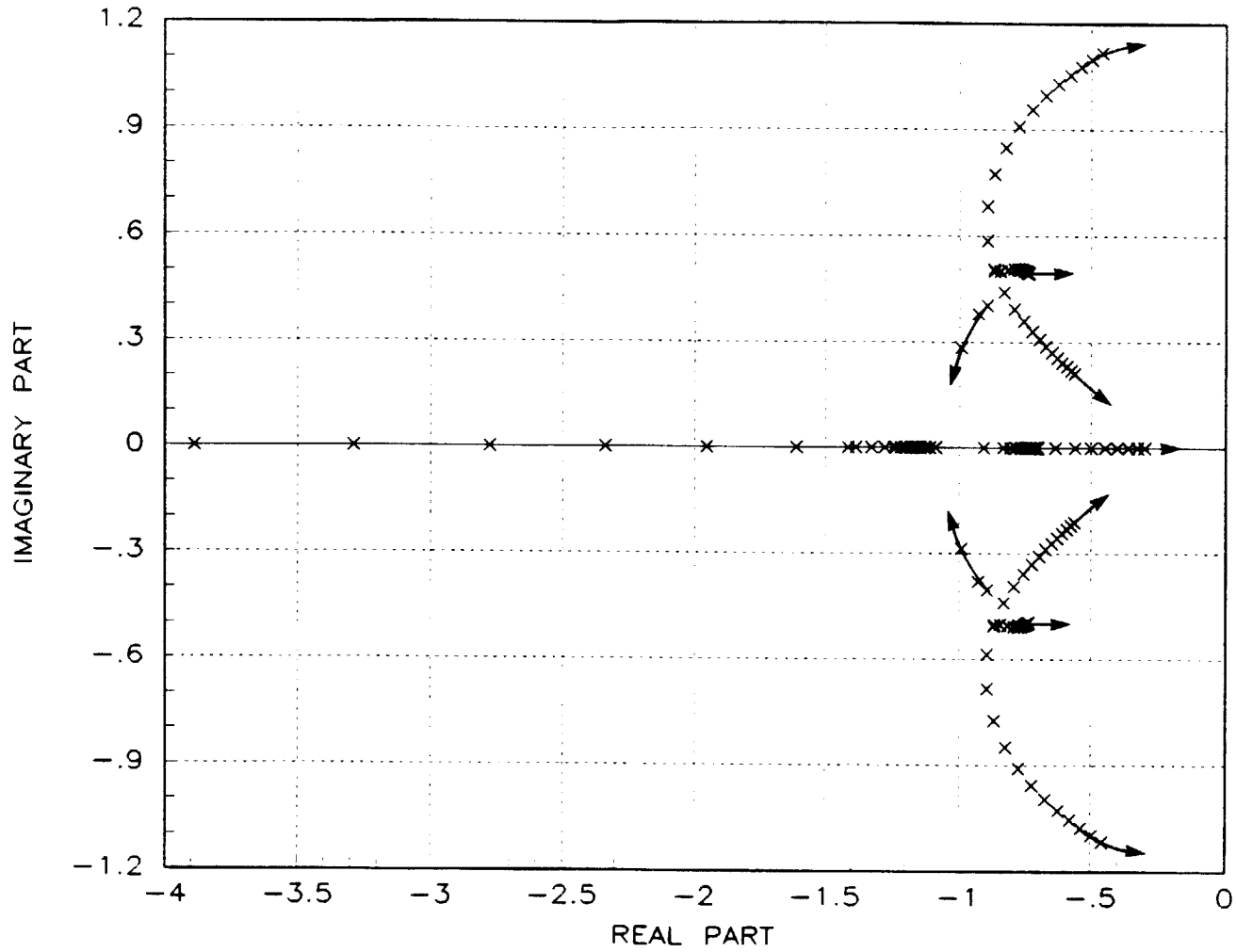


Figure 27.-Low frequency eigenvalues of figure 26.

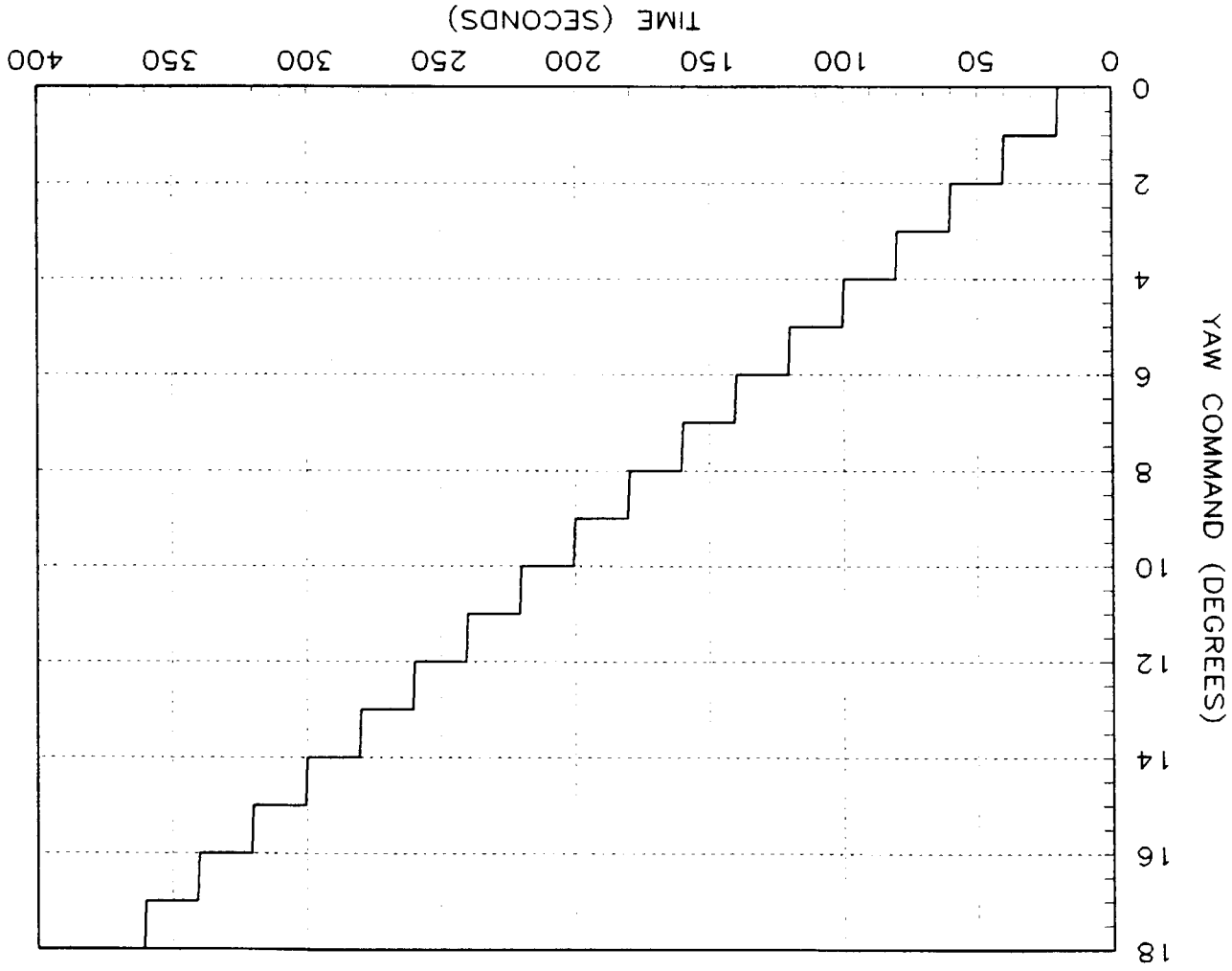


Figure 28.-Input to discrete integral feedback regulator with feedback gains calculated at zero yaw angle.

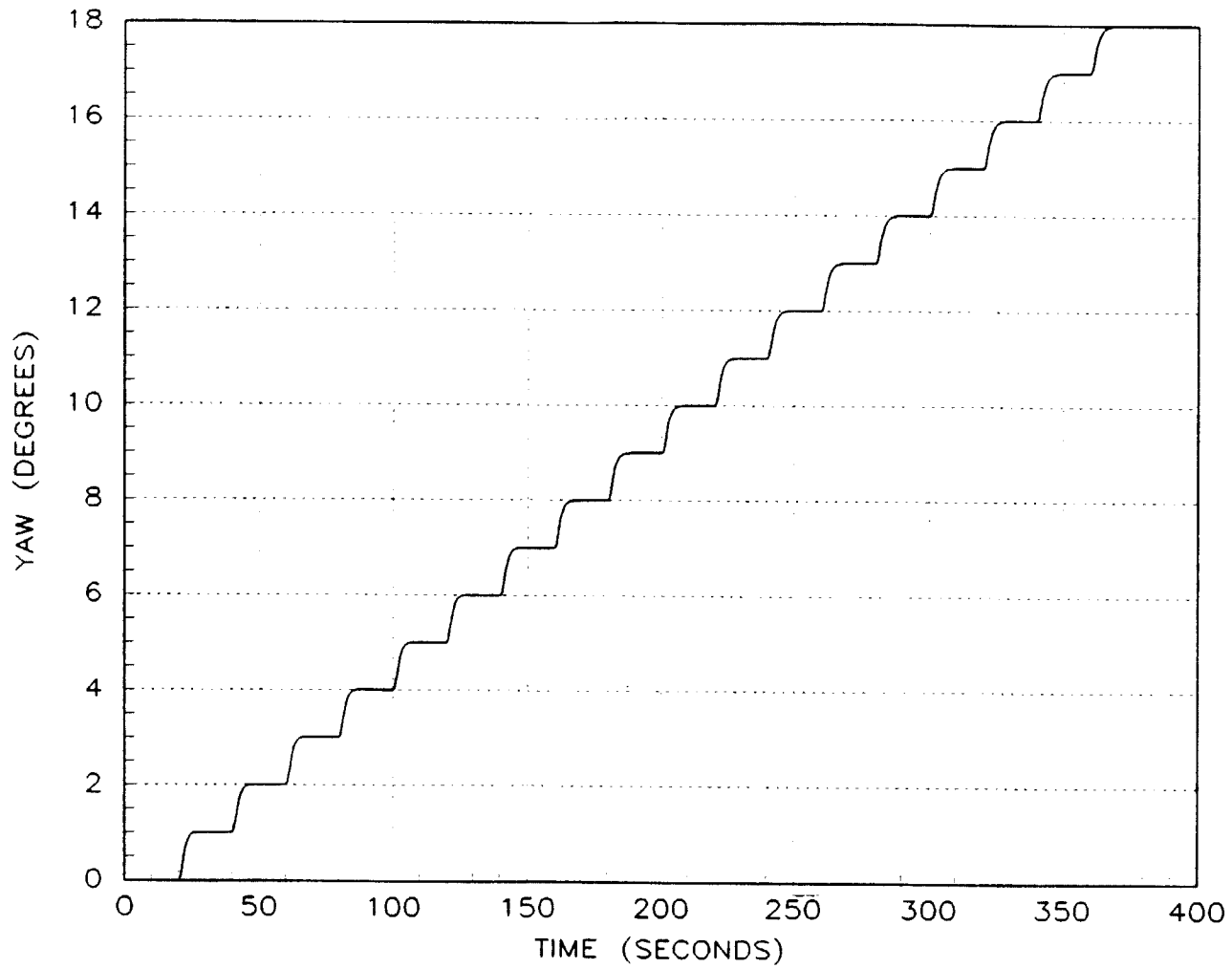


Figure 29.-Yaw angle response to command input of figure 28.

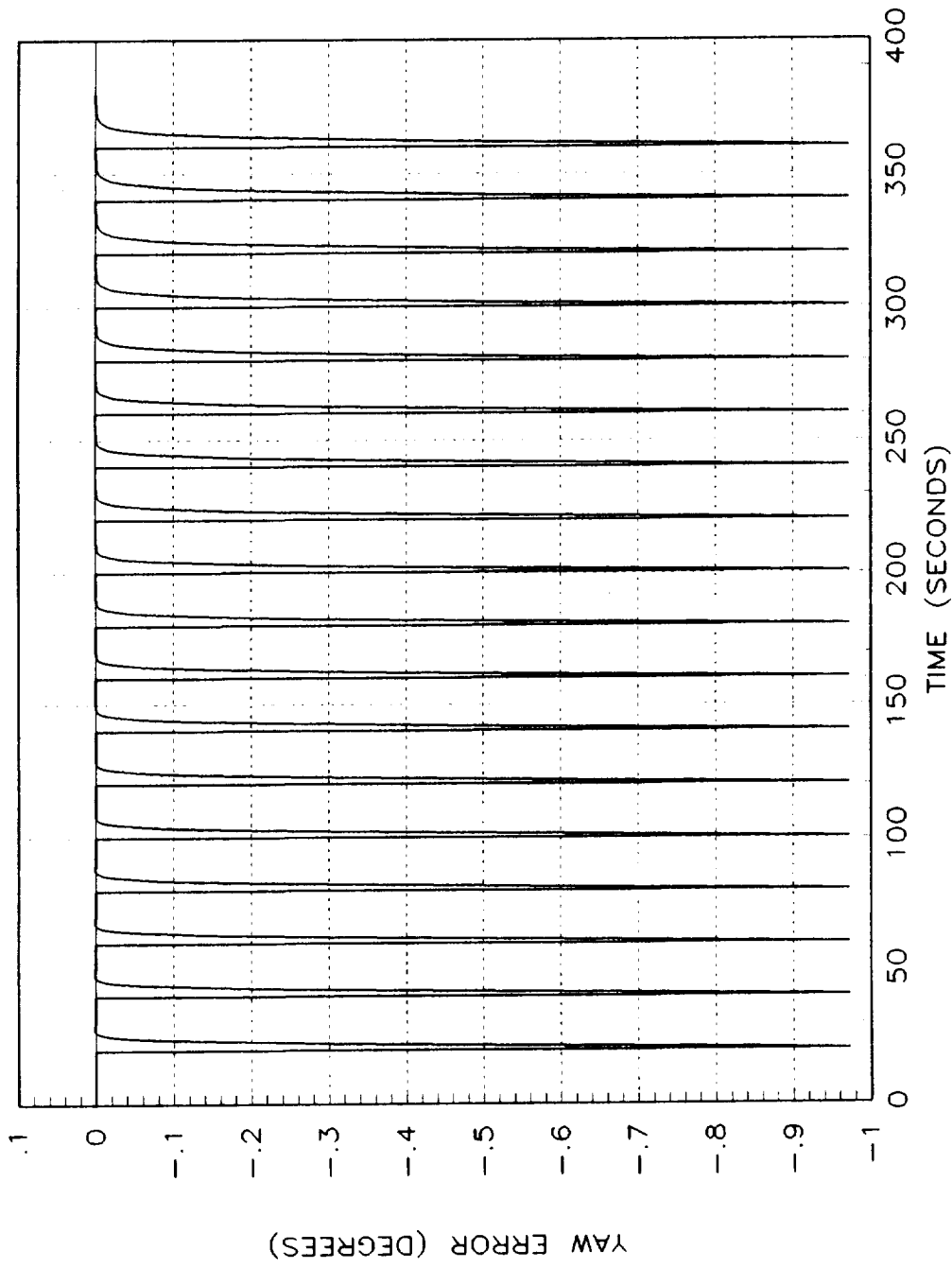


Figure 30.-Difference between command input of figure 28 and response of figure 29.

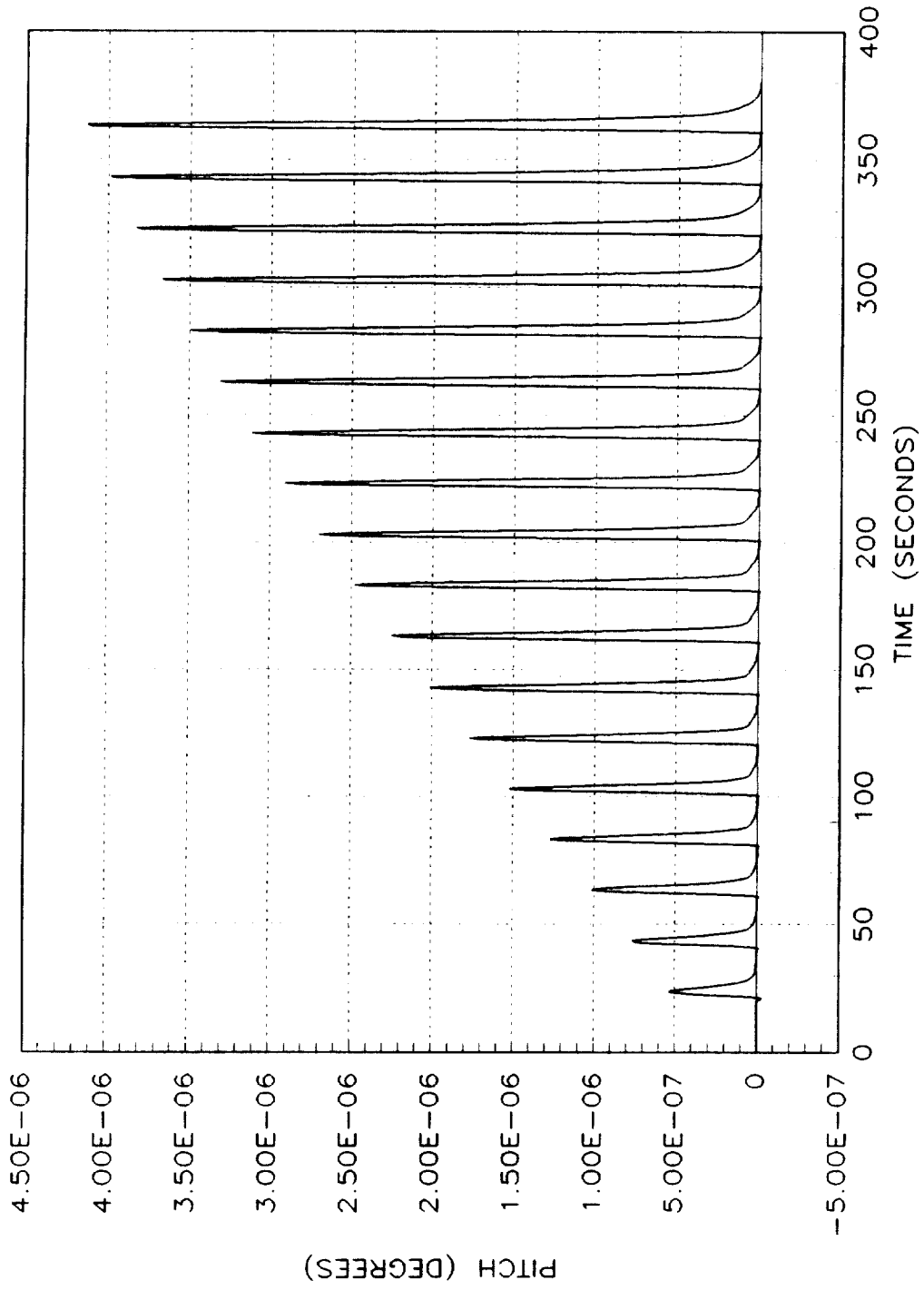


Figure 31 .-Pitch angle response to command input of figure 28.

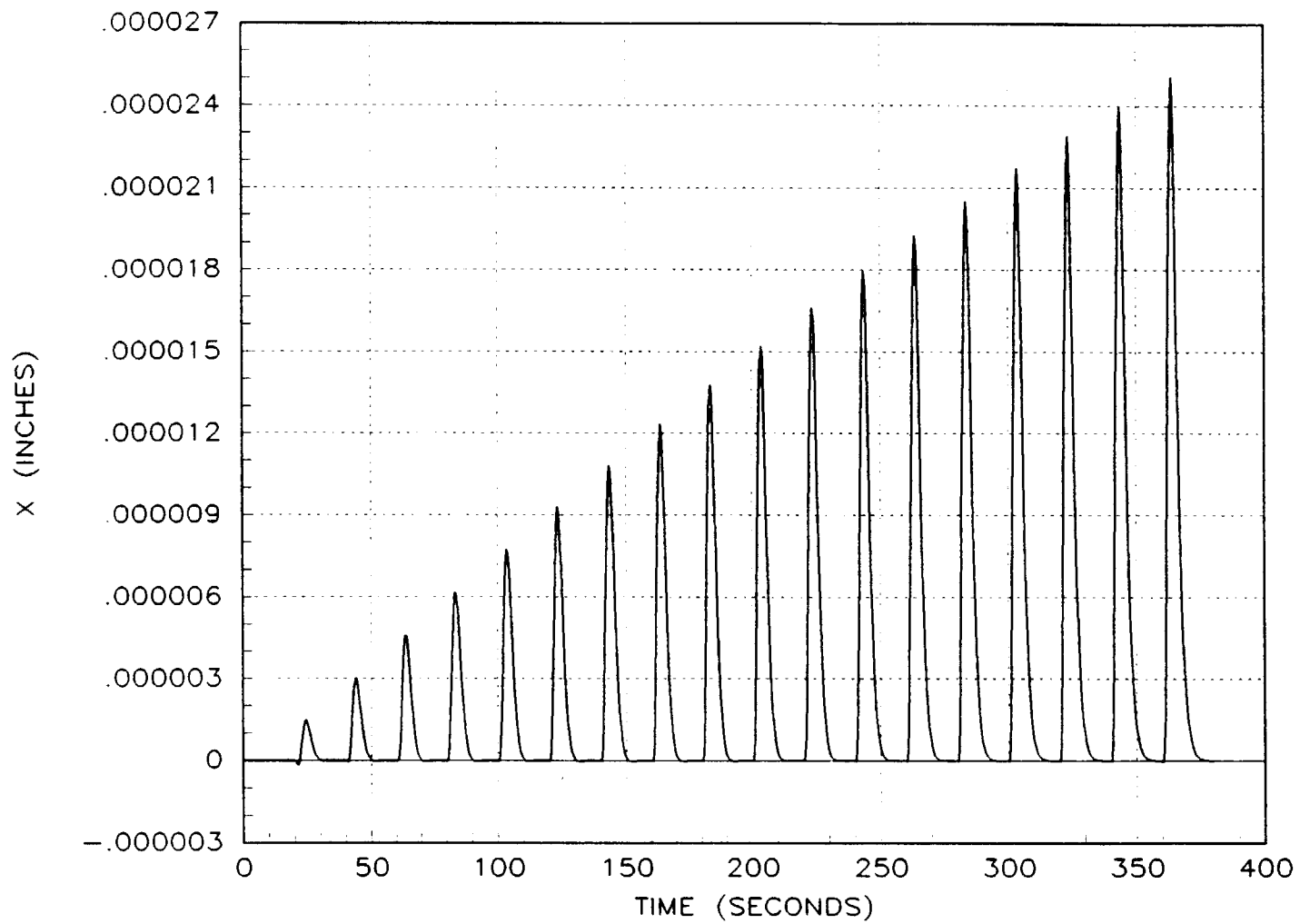


Figure 32.-X axis translational response to command input of figure 28.

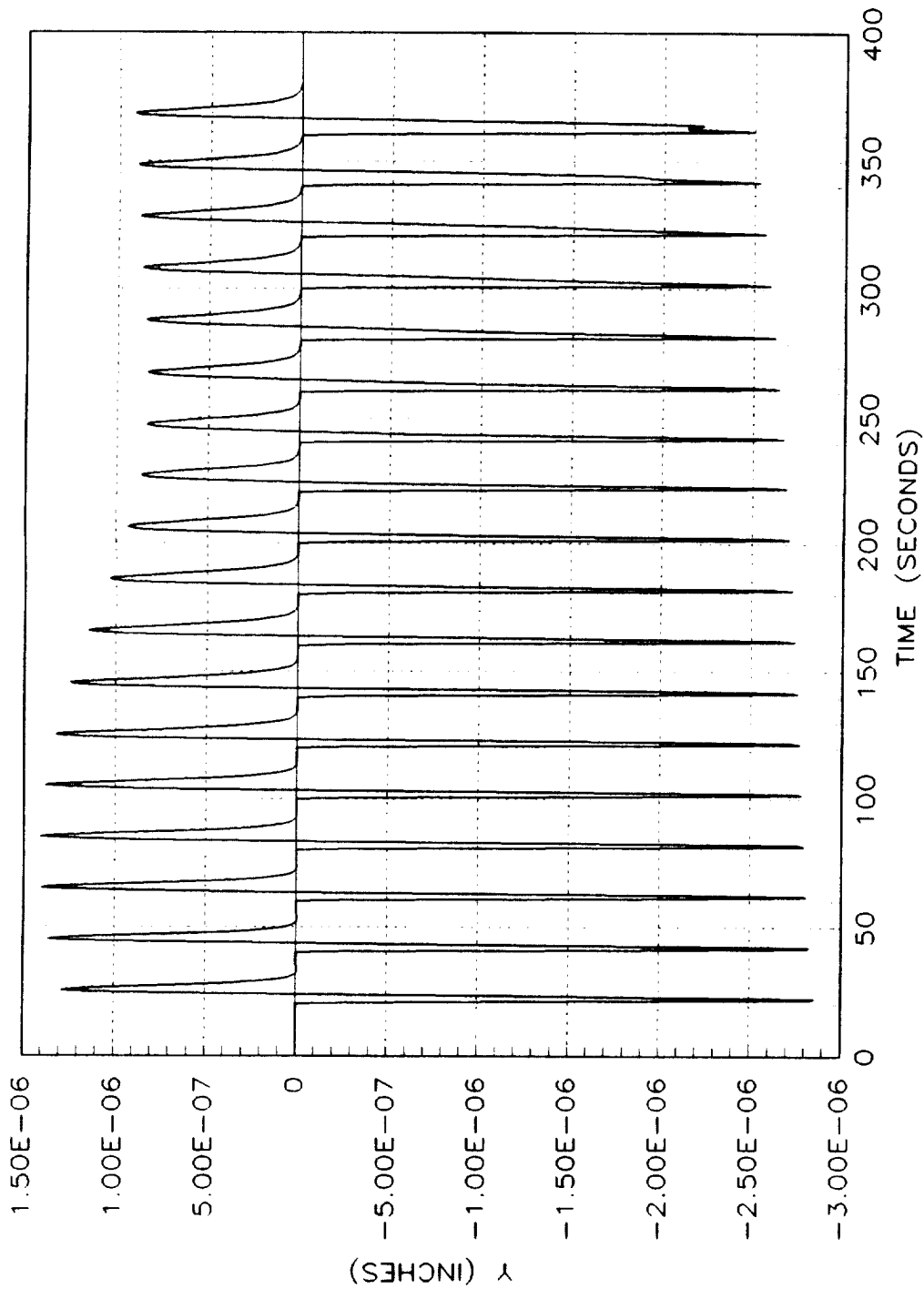


Figure 33.-Y axis translational response to command input of figure 28.

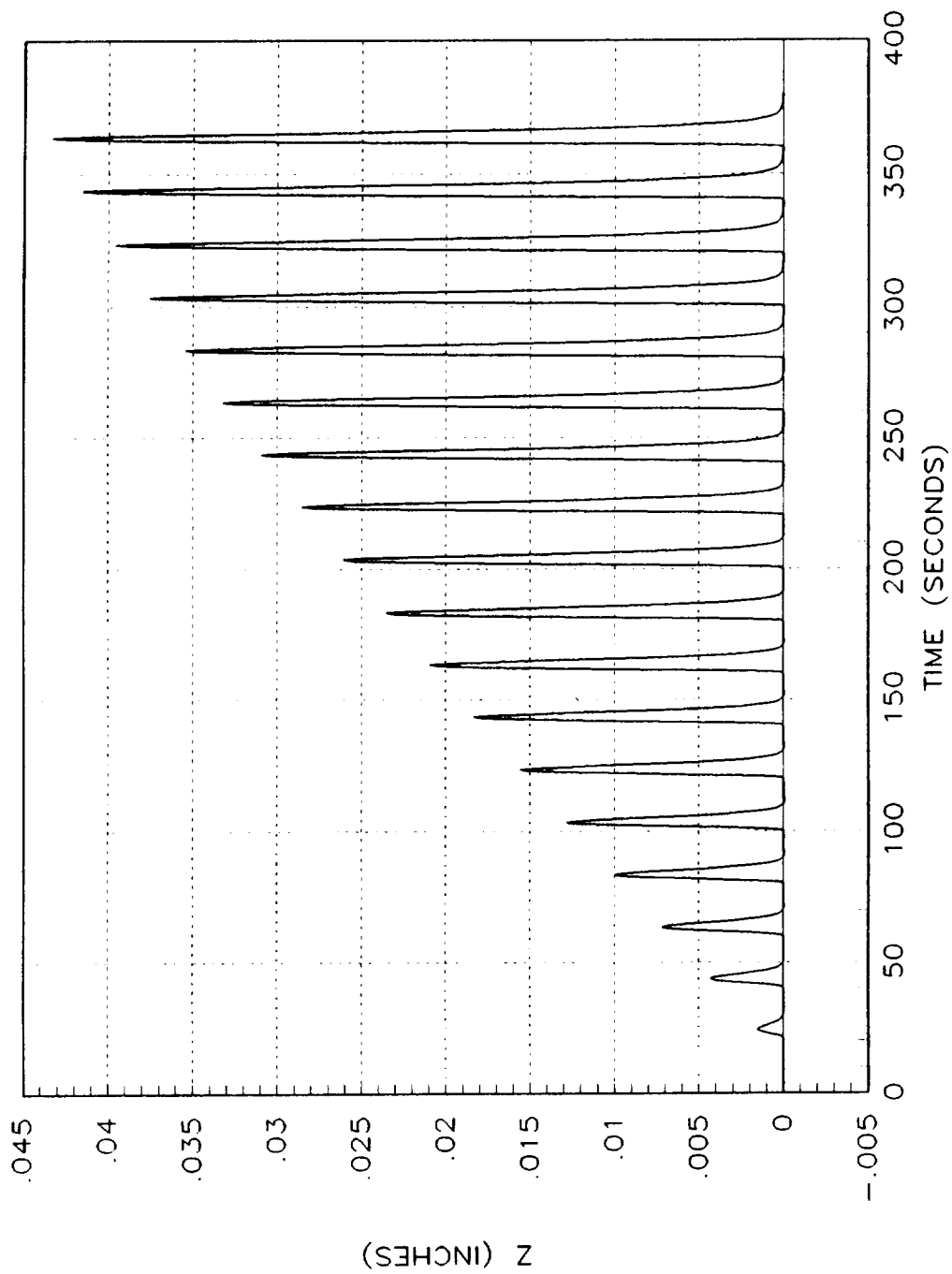


Figure 34 .-Z axis translational response to command input of figure 28.



Report Documentation Page

1. Report No. NASA TM-101606	2. Government Accession No.	3. Recipient's Catalog No.	
4. Title and Subtitle An LQR Controller Design Approach for a Large Gap Magnetic Suspension System (LGMSS)		5. Report Date July 1990	6. Performing Organization Code
		8. Performing Organization Report No.	
7. Author(s) Nelson J. Groom and Philip R. Schaffner		10. Work Unit No. 505-66-91-02	
9. Performing Organization Name and Address NASA Langley Research Center Hampton, VA 23665-5225		11. Contract or Grant No.	
		13. Type of Report and Period Covered Technical Memorandum	
12. Sponsoring Agency Name and Address National Aeronautics and Space Administration Washington, DC 20546-0001		14. Sponsoring Agency Code	
		15. Supplementary Notes	
16. Abstract Two control approaches for a Large Gap Magnetic Suspension System (LGMSS) are investigated and numerical results are presented. The approaches are based on Linear Quadratic Regulator (LQR) control theory and include a nonzero setpoint regulator with constant disturbance input and an integral feedback regulator. The LGMSS which is considered provides five degree of freedom control. The suspended element is a cylinder which is composed of permanent magnet material and the magnetic actuators are air core electromagnets mounted in a planar array.			
17. Key Words (Suggested by Author(s)) Magnetic Suspension; Magnetic Levitation; Pointing System; Magnetic Suspension Model; Magnetic Suspension Control System		18. Distribution Statement Unclassified - Unlimited Subject Category 31	
19. Security Classif. (of this report) Unclassified	20. Security Classif. (of this page) Unclassified	21. No. of pages 64	22. Price A04